

AD-A100 813

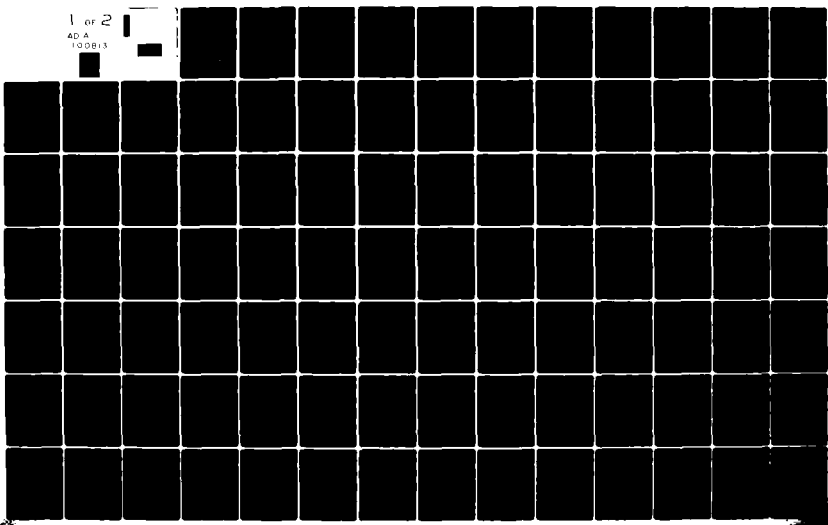
AIR FORCE INST OF TECH WRIGHT-PATTERSON AFB OH SCHOO--ETC F/G 10/2  
THE EFFECT OF ROTOR GEOMETRY ON THE HARMONIC PERFORMANCE OF SYN--ETC(U)  
DEC 80 C STUERKE, D W NORDQUIST

UNCLASSIFIED

AFIT/GE/EE/80D-34

NL

1 or 2  
AD-A  
100013



14

AFIT/GE/EE/80D-34

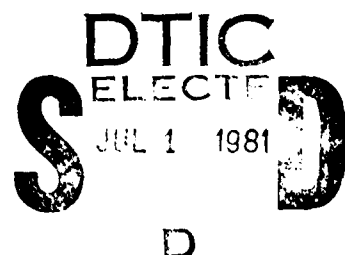
Accession For	
NTIS GRA&I	<input checked="" type="checkbox"/>
DTIC TAB	<input type="checkbox"/>
Unannounced	<input type="checkbox"/>
Justification	
By _____	
Distribution/ _____	
Availability Codes	
Dist	Avail and/or Special
A	

THE EFFECT OF ROTOR GEOMETRY  
ON THE HARMONIC PERFORMANCE OF  
SYNCHRONOUS GENERATORS

THESIS \*

AFIT/GE/EE/80D-34

Cecil Stuerke      David W. Nordquist  
Captain USAF      Captain USAF



Approved for public release; distribution unlimited.

THE EFFECTS OF ROTOR GEOMETRY  
ON THE HARMONIC PERFORMANCE OF  
SYNCHRONOUS GENERATORS

THESIS

Presented to the Faculty of the School of Engineering  
of the Air Force Institute of Technology  
Air Training Command  
in Partial Fulfillment of the  
Requirements for the Degree of  
Master of Science

by

Cecil Stuerke, B.S.

Captain USAF

Graduate Electrical Engineering

December 1980

David W. Nordquist, B.S.

Captain USAF

Approved for public release; distribution unlimited.

## Preface

In the Air Force, there is a strong need for the lightest weight electrical generator with the highest possible efficiency. This brought about a thesis topic. In the topic it was proposed that two students investigate the effects of rotor geometry on improving the harmonic performance of a synchronous generator. If the harmonic performance could be improved enough, it was hoped that wave shaping circuitry external to the generator could be eliminated.

We chose this thesis topic because of the depth of our early graduate courses in power systems and our keen desire to increase our knowledge in this area.

We would like to thank Dr. Frederick Brockhurst for his guidance throughout all stages of this thesis effort. We would also like to thank Mr. James Kummeth for his assistance on the Finite Element analysis computer work.

Cecil Stuerke

David W. Nordquist

## Contents

	<u>Page</u>
Preface . . . . .	ii
List of Figures . . . . .	v
List of Tables . . . . .	vi
List of Symbols . . . . .	vii
Abstract . . . . .	xi
I. Introduction . . . . .	1
Background . . . . .	1
Problem and Scope . . . . .	4
Assumptions . . . . .	5
Approach and Presentation . . . . .	5
II. Theory . . . . .	7
III. Phase Voltage and Current Wave Shapes . . . . .	13
Voltage . . . . .	13
Voltage Example . . . . .	18
Current . . . . .	21
Current Example . . . . .	21
IV. Armature Reaction . . . . .	26
Single-Phase Winding . . . . .	26
Distribution Example . . . . .	29
Polyphase Windings . . . . .	29
Example . . . . .	30
V. Rotor MMF . . . . .	33
Example . . . . .	35
VI. Total MMF . . . . .	37
Example . . . . .	38

	<u>Page</u>
VII. MMF Cancellation . . . . .	40
Armature Reaction MMF . . . . .	40
Example . . . . .	43
Comparison . . . . .	44
VIII. Reluctance Harmonic Control . . . . .	46
Flux Density . . . . .	46
Reluctance Specification Concept . . . . .	48
Methodology . . . . .	50
Example . . . . .	51
How Many Harmonics. . . . .	55
The Contradiction . . . . .	56
IX. Incremental Reluctance Specification . . . . .	58
MMF to Flux Density . . . . .	58
Reluctance Specification . . . . .	59
Example . . . . .	60
Triangular Phase Voltage Wave Shape Example .	61
X. Other Magnetic Effects . . . . .	68
Introduction . . . . .	68
Leakage Flux . . . . .	69
Fringing Flux . . . . .	70
Magnetic Saturation . . . . .	71
Finite Element Analysis . . . . .	71
XI. Conclusions and Recommendations . . . . .	75
Conclusions . . . . .	75
Recommendations . . . . .	76
Bibliography. . . . .	79
Appendix I: Sample Generator . . . . .	81
Appendix II: RGRID and TRIA Card Generation . . . . .	85
Vita: Captain Stuerke . . . . .	106
Vita: Captain Nordquist . . . . .	107

## List of Figures

<u>Figure</u>		<u>Page</u>
1	Full Wave Bridge Rectifier . . . . .	2
2	One Pole of the Rotor and the Stator . . . . .	10
3	Phase Circuit Impedance . . . . .	14
4	Phase Voltage Wave Shape Examples . . . . .	16
5	Time Variation of the Chosen Internal Phase Voltage and Flux Density . . . . .	20
6	Equivalent Circuit During Commutation . . . . .	23
7	Time Variation of the Chosen Phase Current . . . .	24
8	Reluctance Harmonic Control Example Wave Shapes	54
9	Triangular Phase Voltage and Current Wave Shapes	67
10	Sample Generator Mesh Plot . . . . .	74
11	Cross Section of the Sample Generator (Specifications and Dimensions) . . . . .	84
12	Cross Section of the Sample Generator (RGRID and TRIA Cards) . . . . .	87

List of Tables

<u>Table</u>		<u>Page</u>
1	Normalized Current in Six Internal Phases versus Time . . . . .	25
2	Normalized Spacial Component of Armature Reaction, $K(x,r)$ , at Slots of Phase C (Figure 2) . . . . .	30
3	Normalized Total Armature Reaction MMF at Slots of Phase C . . . . .	32
4	Rotor MMF . . . . .	36
5	Total MMF at Phase C Slots versus Time . . . . .	39
6	Space Harmonic Indexes for Armature Reaction Traveling Waves . . . . .	44
7	Normalized Phase Current and Voltage (Triangle Wave Shape) (Figure 9a) . . . . .	63
8	Normalized Armature Reaction MMF, Phase C Slots (Triangle Wave Shape) . . . . .	64
9	Total MMF at Phase C Slots (Triangle Wave Shape) . . . . .	65
10	Calculation of Incremental Reluctances (Triangle Wave Shape) . . . . .	66
11	Sample Generator Dimensions and Specifications.	83

## List of Symbols

### Greek Letter Symbols

$\alpha_e$  - Electrical angle between slots (electrical radians)  
 $\delta$  - Air gap distance (meters)  
 $\Delta$  - Incremental change  
 $\infty$  - Infinity  
 $\lambda$  - Electrical angle of skew (electrical radians)  
 $\mu$  - Magnetic permeability (henries/meter)  
 $v$  - Space harmonic number  
 $\omega$  - Frequency (hertz or radians/second)  
 $\pi$  - The constant Pi, 3.1415926535 .....

$\phi$  - Magnetic flux (webers)  
 $T_p$  - First harmonic rotor pole pitch (radians or slots)

### Roman Letter Symbols

A - Internal generator phase  
A - External generator phase  
A' - Internal generator phase  
AC - Alternating current  
 $A_{gv}$  - Constant defined in Equation (26)  
 $a$  - area ( $\text{meters}^2$ )  
 $a_g$  - Coefficient of the Fourier series expansion of the phase current sine terms  
B - Internal generator phase  
B - External generator phase  
B - Magnetic flux density magnitude (webers/ $\text{meter}^2$ )

### List of Symbols

#### Roman Letter Symbols (continued)

B' - Internal generator phase

$B_{gv}$  - Constant defined in Equation (32)

$B_{max}$  - Maximum amplitude of the magnetic flux density  
(webers/meter<sup>2</sup>)

$B_{TOT}$  - Total magnetic flux density (webers/meter<sup>2</sup>)

$B_x(t)$  - Magnetic flux density at location x versus time  
(webers/meter<sup>2</sup>)

$b_g$  - Coefficient of the Fourier series expansion of  
the phase current cosine terms

$b_p$  - Rotor pole arc (radians or slots)

$b_v$  - Coefficient of the Fourier series expansion of the  
flux density space variation sine terms

C - Internal generator phase

C' - External generator phase

$C_n$  - Centers of reluctance increments on the rotor

DC - Direct current

d - Incremental width (seconds)

g - Time harmonic number

$I_F$  - Rotor current (amperes)

$I(t)$  - Generator phase current versus time (amperes)

$I_{max}$  - Maximum generator phase current (amperes)

K - A proportionality constant defined in Equation (40)

## List of Symbols

### Roman Letter Symbols (continued)

$K(t, r)$  - Time MMF Variation  
 $K(x, r)$  - Space MMF variation  
 $K_{pv}$  -  $v$ th harmonic pitch factor  
 $K_{dv}$  -  $v$ th harmonic distribution factor  
 $K_{sv}$  -  $v$ th harmonic skew factor  
 $k$  - Integer constant  
 $\ell_m$  - Magnetic path length (meters)  
 $\ell$  - Effective rotor length (meters)  
MMF - Magnetomotive force (ampere-turns)  
 $MMF_x(t)$  - MMF at location  $x$  versus time (ampere-turns)  
 $MMF_{max}$  - Maximum MMF as defined in Equation (18) (ampere-turns)  
 $MMF_{rotor}$  - Rotor MMF (ampere-turns)  
 $MMF(x, t)$  - MMF as a function of distance and time (ampere-turns)  
 $MMF(x)$  - MMF versus distance - the space variation only (ampere-turns)  
 $MMF^*(t)$  - MMF reflected into the first slot (ampere-turns)  
 $m$  - Total number of internally generated phases  
 $n$  - Stator slot number  
 $q$  - Width of a phase belt (slots)  
 $R$  - Reluctance (henries<sup>-1</sup>)  
 $R_L$  - Load resistance (ohms)  
 $RMS$  - Root-Mean-Square

### List of Symbols

#### Roman Letter Symbols (continued)

$R_x(t)$  - Reluctance at location  $x$  versus time (henries $^{-1}$ )

$r$  - Individual internal generator phase

$s$  - Number of turns of a coil group in a single stator slot

$s_r$  - Rotor coil turns

$T$  - Period of a given waveform

$t$  - Time (seconds)

$v_{ang}$  - Rotor angular velocity (radians/seconds)

$v$  - Rotor tip velocity (meters/second)

$v_{coil}$  - Coil or coil group voltage (volts)

$v_\ell$  - Load voltage (volts)

$v_g$  - Internally generated line to line voltage (volts)

$w$  - Winding pitch (radians or slots)

$x$  - Distance along the circumference of the inside of the stator in stator coordinates (meters)

$x'$  - Distance along the circumference of the rotor in rotor coordinates (meters)

$z_g$  - Generator impedance (ohms)

$z_T$  - Transmission line impedance (ohms)

$z_L$  - Load impedance (ohms)

Abstract

The use of rotor geometry as a specification in the control of generator voltage and flux density harmonics is studied. The possibility of generating a specific voltage waveform at the load with only a three-phase rectifier between the AC generator and the load is investigated.

Since the specified load voltage is DC, the internally generated phase voltage waveform must be one which keeps constant the greatest instantaneous potential difference between any two phases.

The armature reaction MMF is expressed as an infinite set of traveling waves (with respect to the stator) with an infinite set of velocities. It is shown that the rotor MMF cannot cancel armature reaction everywhere because the rotor MMF has only the velocity of the rotor (not an infinite set of velocities).

The MMFs present at all the stator slots of an armature coil group are reflected into a single slot in an attempt to control the air gap flux density harmonics by selectively positioning increments of rotor reluctance. This method fails because a general solution for the reflected flux densities (appropriately synchronized with each other) could not be obtained. This method can be further investigated if such a general solution can be found.

Specifying the air gap reluctance incrementally as the rotor moves under successive stator slots is also tried as a means of harmonic control. This method proves unworkable due to negative MMF requirements and conflicting geometry specifications.

Finite Element analysis is introduced as a computer aid to the design of a magnetic structure. A specific computer program, MAGNETIC, is introduced. Another computer program is developed which generates input data for MAGNETIC. This input data is for the pole shoe and air gap regions of the generator. The program allows for a variable air gap shape.

Recommendations are included which may allow the successful specification of rotor geometry as a means of harmonic control, or which may prove the concept impossible.

THE EFFECTS OF ROTOR GEOMETRY  
ON THE HARMONIC PERFORMANCE OF  
SYNCHRONOUS GENERATORS

I. Introduction

Background

For more than a decade, synchronous AC generators have been used to supply power to loads that require other than a pure sinusoidal AC voltage. The circuit configuration of a typical example is shown in Figure 1.

The AC generator, also called an alternator, allows sliprings to replace troublesome DC generator commutators. In the case of brushless AC generators, sliprings are even eliminated. In high voltage applications, AC generators have the additional advantages of a more easily insulated stationary armature (Ref 6:336).

In order to supply a non-sinusoidal voltage, a conventional AC generator requires external wave shaping circuitry. A DC load voltage requires that the AC generator output be rectified and also requires a large filter. A DC generator application may use a smaller filter, but this does not outweigh the commutator disadvantage.

The relative simplicity, reliability, and insensitivity to wear, corrosion, and breakage make AC generators beneficial even in DC applications (Ref 2:76) and (Ref 7). An AC generator with a tailored voltage output adds to these advantages.

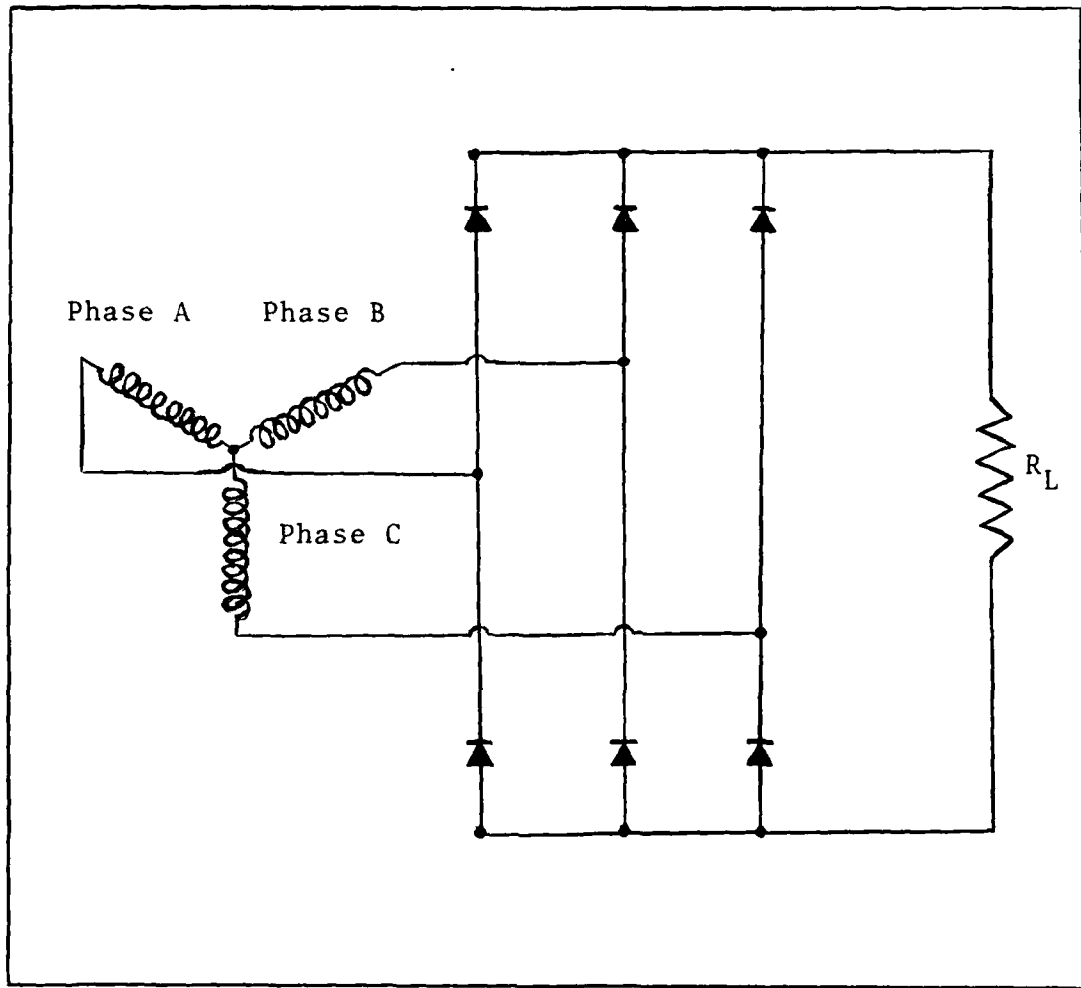


Figure 1 Full Wave Bridge Rectifier

The voltage in each AC generator coil varies in time, but is not automatically sinusoidal. The voltage wave shape depends on the magnetic flux density field in the generator's air gap. The field is distorted due to the effects on salient pole geometry, conductor slots, and armature reaction. The time variation of the distorted voltage wave shape may be resolved into the sum of fundamental and higher order Fourier components.

The harmonics of the voltage time variation must be controlled. The first few harmonics contain significant power that the prime mover must supply. If the power from some of these harmonics must be trimmed from the load, it is generally dissipated as wasted heat in a conventional generator and filter circuit. Without proper control, the voltage wave shape inside the generator may have peaks that require increased armature insulation. An undesirably large and heavy generator is required to solve the preceding problems.

Conventional generator design includes methods for harmonic control. Generator geometry is normally used to suppress the most significant undesired harmonics. Specification of the distribution, pitch, and skew of the armature coils as well as the rotor pole arc provides a direct and effective means of harmonic control. If the wave shape can be trimmed to its fundamental component, the analysis necessary to

shape the waveform to the needs of the load is much easier. For any waveform, the shaping amounts to the reintroduction of properly sized higher harmonics at the expense of the fundamental.

When the generator is dedicated to specific load which requires other than the fundamental frequency voltage and current, the conventional design procedure is a disservice. If the voltage wave shape is obtained directly at the generator terminals, it is possible to meet the load power requirements with a smaller filter and at the same time reduce generator losses. Rotor geometry control can help provide the correct voltage at the generator terminals.

#### Problem and Scope

The purpose of this thesis effort is to investigate the possibility of generating a specific DC voltage waveform at the load with only a rectifier between the AC generator and the load. Rotor geometry modifications are to be investigated as the main means of control. This control method is applied to the generation of specific phase voltages (by controlling generator flux density harmonics) that will yield the desired load voltage using only rectification to modify the voltage wave shape. This effort reviews the theory by which rotor geometry and the voltage wave shape are related. From this basis, processes for determining a satisfactory rotor geometry are studied.

### Assumptions

The attempts at rotor geometry determination through required reluctance do not account for the effects of finite permeability or flux fringing in the generator magnetic structure. These effects are considered negligible, but are discussed as they are observed in the finite element analysis (Section X). The basic generator design and the load parameters used in the development of numerical examples are assumptions taken from the generator design covered in Appendix I.

### Approach and Presentation

Section I is an introduction. Section II reviews the theory through which the generator magnetic flux density is related to rotor geometry. This provides the basis for harmonic control.

In Section III, the load voltage requirements are used to select the waveform of the phase voltage and current. The specification of the phase voltage waveform determines the required magnetic flux density versus time in the generator. The specification of the phase current allows calculation of the armature reaction. Armature reaction MMF (magnetomotive force) is calculated in Section IV.

Section V develops an expression for the rotor MMF. Section VI combines the armature reaction and rotor MMF in an expression for the MMF at the slots of a phase group versus time. An example is included.

Section VII discusses the limitations in the use of rotor MMF to cancel certain harmonics of armature reaction.

Section VIII describes an attempt to control the flux density harmonics with the introduction of selectively positioned increments of rotor reluctance. Reasons for the inapplicability of this approach are discussed.

Section IX describes the incremental specification of rotor reluctance as it is rotated into position under an armature coil. The insufficiency of this approach is also discussed.

Section X looks at the effects of finite permeability and flux fringing. Finite Element analysis is shown to be an excellent tool in fine tuning generator design to account for these effects.

Section XI recommends other approaches to the solution of the harmonic control problem for further research.

## II. Theory

This section reviews the theory through which the generator magnetic flux density is related to rotor geometry. This discussion provides a basis for the control of the flux density harmonics.

In electromechanical energy conversion, the magnetic field is the intermediate stage. A rotating generator shaft causes magnetic lines of flux generated by the rotor coils to cut the armature coils. A voltage is induced in each coil according to Faraday's Law

$$V_{\text{coil}} = -d\phi / dt \quad (1)$$

where

$V_{\text{coil}}$  is the instantaneous induced voltage

$\phi$  is the magnetic flux in webers

$t$  is the time in seconds

The coil voltages combine as coil group voltage which combine as phase in voltages. The phase voltages are rectified to provide the load voltage.

"At a particular rotating speed, the instantaneous volts per conductor are proportional to the air gap flux density at the conductor. The wave shape of the conductor voltage versus time is therefore the same as that of the air gap flux density vs distance around the periphery." (Ref 3: Chap 6,6)

The phase voltage is shaped by both the flux density and the layout connection of the armature coils.

The shape of the flux density versus distance may be described as the sum of harmonic components. Each component contributes to the phase voltage. The stator coil's pitch, distribution, and skew determine multiplier factors which modify the voltage (Ref 5:44-55).

When the coil width is less than the width of a rotor pole, its voltage is modified by a pitch factor.

$$K_{pv} = \sin \left( \frac{v\pi}{2} - \frac{W}{T_p} \right) \quad (2)$$

where

$K_{pv}$  is the  $v$ th harmonic pitch factor

$v$  is the space harmonic number being considered

$W$  is the winding pitch in radians or slots

$T_p$  is the first harmonic rotor pole pitch in radians or slots

When the coils are not concentrically placed, the voltage is modified by a distribution factor.

$$K_{dv} = \frac{\sin(v\pi/m)}{q \sin(v\pi/qm)} \quad (3)$$

where

$K_{dv}$  is the  $v$ th harmonic distribution factor

$q$  is the width of a phase belt in slots

$m$  is the number of internally generated phases

When the coils are skewed with respect to the rotor axis, the voltage is modified by a skew factor.

$$K_{sv} = \sin \left( \frac{v\lambda/2}{\lambda/2} \right) \quad (4)$$

where

$K_{sv}$  is the  $v$ th harmonic skew factor

$\lambda$  is the angle of skew in electrical radians

The harmonics of the flux density are also controlled by the pole arc of a salient pole generator ( $b_p$  as shown in Figure 2). Reduction of the pole arc reduces leakage flux, but also reduces the magnitude of all the flux density harmonics as well. Unlike coil pitch, distribution, and skew, the actual magnetic field arc is affected by leakage and the level of magnetic flux saturation.

The typical use of the coil placement and pole arc factors is to eliminate certain undesirable flux density harmonics with minimum reduction of the fundamental. However, because these factors may be used to alter the relative magnitude of harmonics without cancellation, they are important in tailoring the phase voltage wave shape.

The flux density and therefore the phase voltage are shaped not only by the position of the current carrying conductors, but also by the geometry of the generator magnetic circuit.

Current in the stator coils and in the rotor coils are both sources of MMF rotating with respect to the stator. The field produced by these MMF sources may be controlled through variation of the magnetic circuit reluctance.

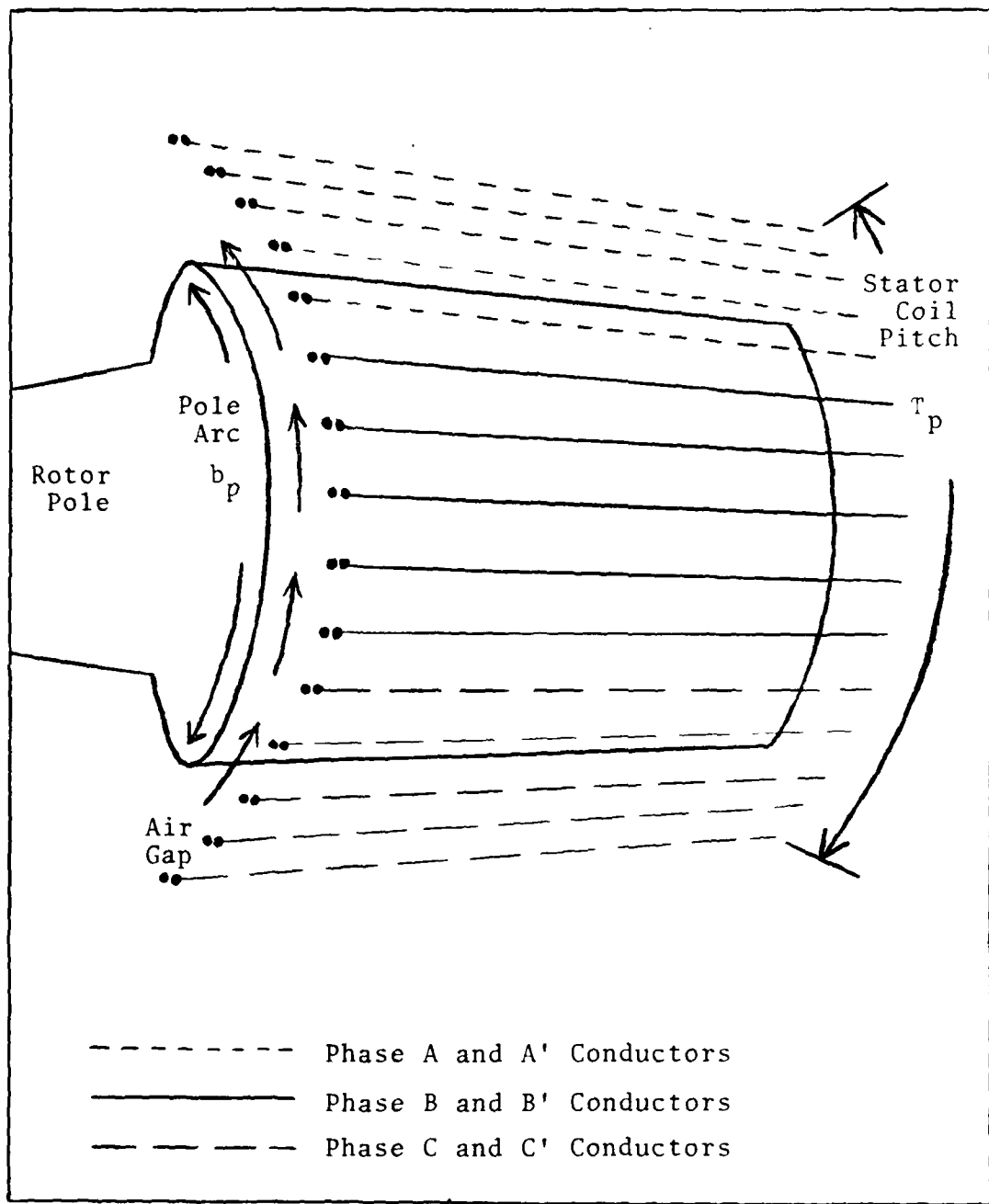


Figure 2 One Pole of the Rotor and the Stator

$$\phi = \text{MMF}/R \quad (5)$$

where

MMF is the magnetomotive force in ampere turns

R is the reluctance in henries<sup>-1</sup>

Reluctance of the magnetic path is:

$$R = \ell_m / \mu a \quad (6)$$

where

$\mu$  is the permeability of the material in henries/meter

$\ell_m$  is the path length in meters

a is the area in meters<sup>2</sup>

Because the permeability for air is much lower than the permeability of the generator steel, the air gap usually dominates the reluctance and the MMF drop around the magnetic circuit. The air gap reluctance (above the rotor) travels with respect to the stator as does the MMF which forces the flux through it.

If both sides of Equation (5) are divided by the area of the flux tube (Ref 1:245), in which the flux is found, it is evident that the flux density is related to the MMF through the length of the flux tube.

$$B = \mu \text{MMF}/\ell_m \quad (7)$$

where

$B$  is the magnetic flux density in webers/meter<sup>2</sup>

When the reluctance is due to the air gap distance, this becomes

$$B = \mu \text{ MMF}/\delta(x) \quad (8)$$

where

$\delta(x)$  is the air gap distance in meters

$x$  is the distance along the circumference of the inside of the stator in meters (stator coordinates)

The chosen method for tailoring the magnetic flux density is first to calculate the MMF variation at each slot, and then to adjust the reluctance through variation of the length of the air gap at the slots. The magnetic flux density in turn produces a phase voltage that becomes the desired voltage wave shape when rectified.

### III. Phase Voltage and Current Wave Shapes

This section presents the theory and the selection of an acceptable phase voltage wave shape. The current wave shape which follows from the voltage is also presented. The load voltage requirement is the basic criteria on which the selections are based.

A number of different phase voltage wave shapes can produce the desired load voltage wave shape after being rectified. Thus, the harmonic content of the generator magnetic field that produces the voltage and current wave shapes is a design option.

#### Voltage

The generator must supply the required load voltage in spite of the generator transmission line impedances. If, as is shown in Figure 3, the load voltage is specified and the impedances are known, the required line to line voltage wave shape may be determined by circuit analysis.

$$v_g = v_\ell + \frac{v_\ell}{z_L} (z_g + z_T) \quad (9)$$

where

$v_g$  is the internally generated line to line voltage

$v_\ell$  is the required load voltage

$z_L$  is the load impedance in ohms

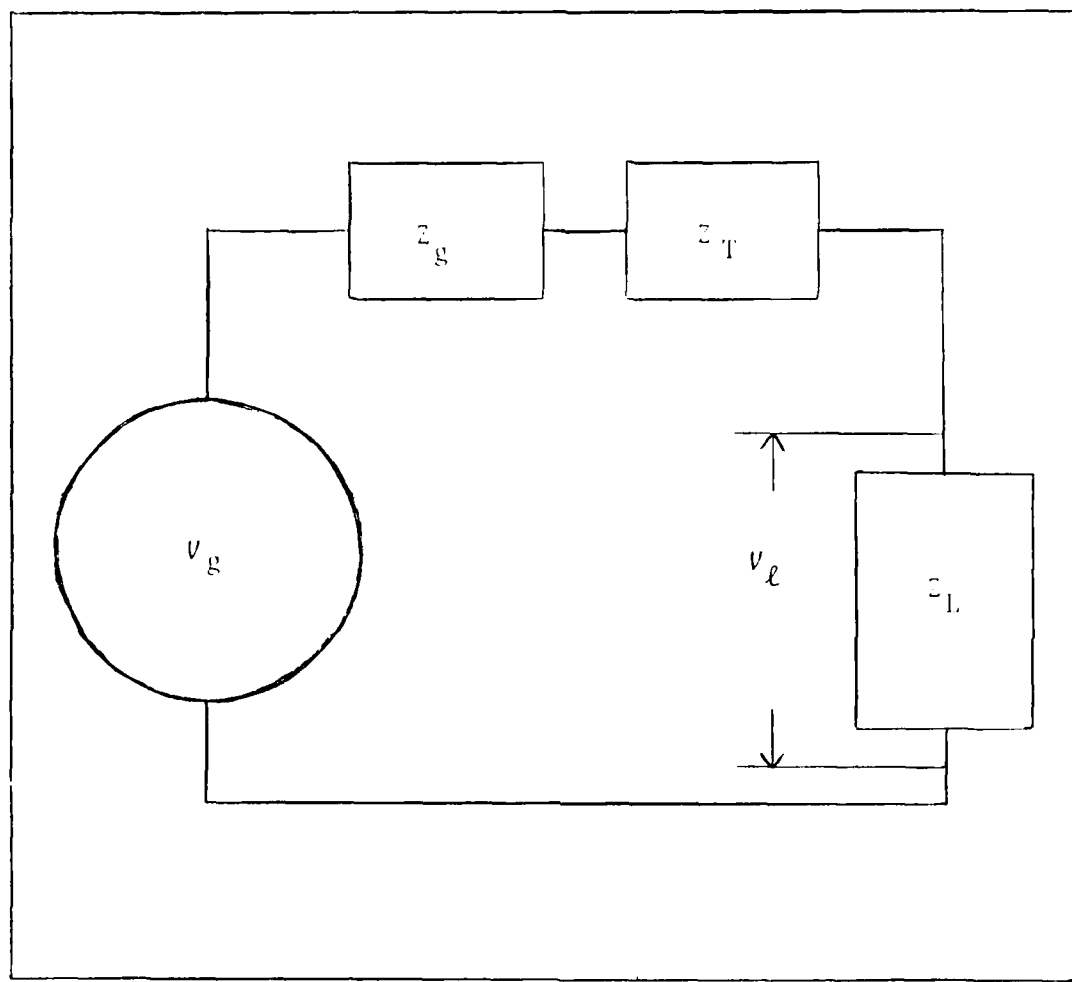


Figure 3 Phase Circuit Impedance

$Z_g$  is the internal generator impedance in ohms

$Z_T$  is the transmission line impedance in ohms

This analysis is to be accomplished harmonic by harmonic from the components of the load voltage. Remember that the impedances are functions of frequency. It is the phase voltage leading to the composite  $V_g$  that must be induced in the armature coils by the aggregate magnetic field.

The shape of the desired load voltage wave shape specifies the phase voltage difference (between any two external generator phases) during the period in which it is applied to the load. This is because the three-phase rectifier applies the greatest instantaneous potential difference between any two phases to the load. If the load voltage is DC, the maximum phase difference is required to be constant. As the voltage in one phase falls below the necessary value, another phase must rise to replace it.

Equally loaded symmetrical phases will have identical voltage wave shapes. Successive phases will be evenly displaced through  $2\pi$  electrical radians of rotor rotation.

Example phase voltage wave shapes which meet the DC load requirements are shown in Figure 4. Notice that in Figure 4c, overlapping voltages are possible. In these cases, current is supplied from more than two phases at a time.

The shape of the phase voltages as they transition is not specified by the load voltage requirements. It is

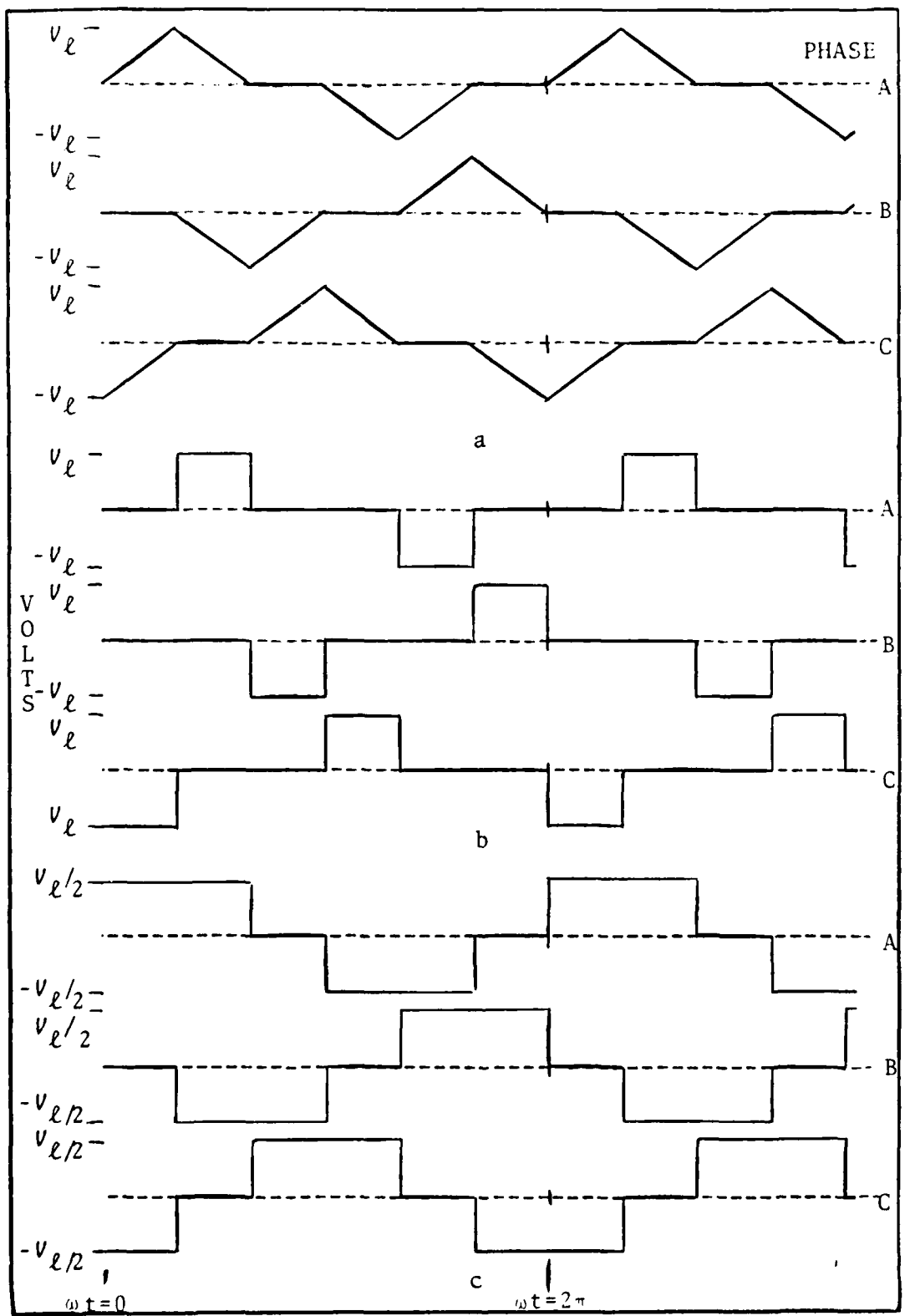


Figure 4 Phase Voltage Wave Shape Examples

unnecessary for the phase voltage transition to encourage proper current commutation because the current in the load is controlled by the applied voltage. The rate of change of the phase voltage may be limited in order to protect the silicon controlled rectifiers and/or diodes used in the three-phase rectifier.

Flexibility in the choice of the phase voltage wave shape is useful because this wave shape must be controlled by a properly engineered magnetic flux density in the air gap.

This flexibility may be exploited under rotor geometry control in order to accomplish flux density control with a minimum mean air gap. This will decrease leakage and improve generator performance. Because the phase voltage determines phase current, its shape also affects the magnetic field shape resulting from the armature reaction.

The shape of the load voltage during its application to the load and its transition affects its harmonic content. The proper choice of the phase voltage wave shape as it is applied to the three-phase rectifier may improve generator performance and/or simplify calculations. Once the effective rotor length, the rotor tip velocity, and the phase voltage are known, the required magnetic flux density is also known.

$$V_{\text{coil}} = Bv\ell \quad (10)$$

where

$V_{coil}$  is the required coil group voltage

$v$  is the rotor tip velocity in meters/second

$\ell$  is the effective rotor length in meters

### Voltage Example

See Appendix I (Generator Design) for a reference on the generator specifications used in this example.

For the example carried through this thesis effort, the desired load voltage is constant (DC). Although the internally generated phase voltage is properly derived from the desired load voltage according to Equation (9), this example begins with the specification of the line to line voltage. The value of the line to line voltage is chosen as 796.74 volts. This is  $\sqrt{3}$  times the RMS phase voltage of the sample sinusoidal AC generator. It is equal to the RMS voltage the generator could supply to a load if it were wye connected and if  $Z_T$  and  $Z_g$  were negligible.

The generator phase voltage output comes from the series connection of four coil groups (two coil groups per pole pair from the generator's two pole pairs). The selected internal phase voltage wave shape is shown in Figure 5. The rectification applies the maximum potential difference between any two external phases to the load. Considering that this difference is across two external phases and considering the

four coil groups in series per external phase, the required coil group voltage is:

$$v_{\text{coil}}^* = 796.74/8 = 99.59 \text{ volts} \quad (11)$$

where

$v_{\text{coil}}^*$  is the peak value of  $v_{\text{coil}}$

The rotor tip speed ( $v$ ) is 119.7 meters/second and the effective rotor length is .6438 meters. The total flux density which the five conductors in each coil group must cut has the same shape versus time as  $v_{\text{coil}}$ . From Equation (10), the maximum flux density is:

$$B_{\max} = \frac{v_{\text{coil}}^*}{v\ell} = 1.292 \text{ webers/meter}^2 \quad (12)$$

where

$B_{\max}$  is the maximum flux density in webers/meter<sup>2</sup>

Figure 5 gives the voltage versus time (external to the generator) for the three phases. Phase B lags phase A internally in the generator by  $\pi/3$  electrical radians (60 electrical degrees). Because phase B is connected in reverse, it lags phase A by an additional  $\pi$  electrical radians (180 electrical degrees) for a total lag of  $4\pi/3$  electrical radians (240 electrical degrees). The flux density for each phase has the same shape as the phase voltage variation.

By Fourier analysis, (Ref 14:Chap 2) the harmonic components of the desired total flux density per phase are given by:

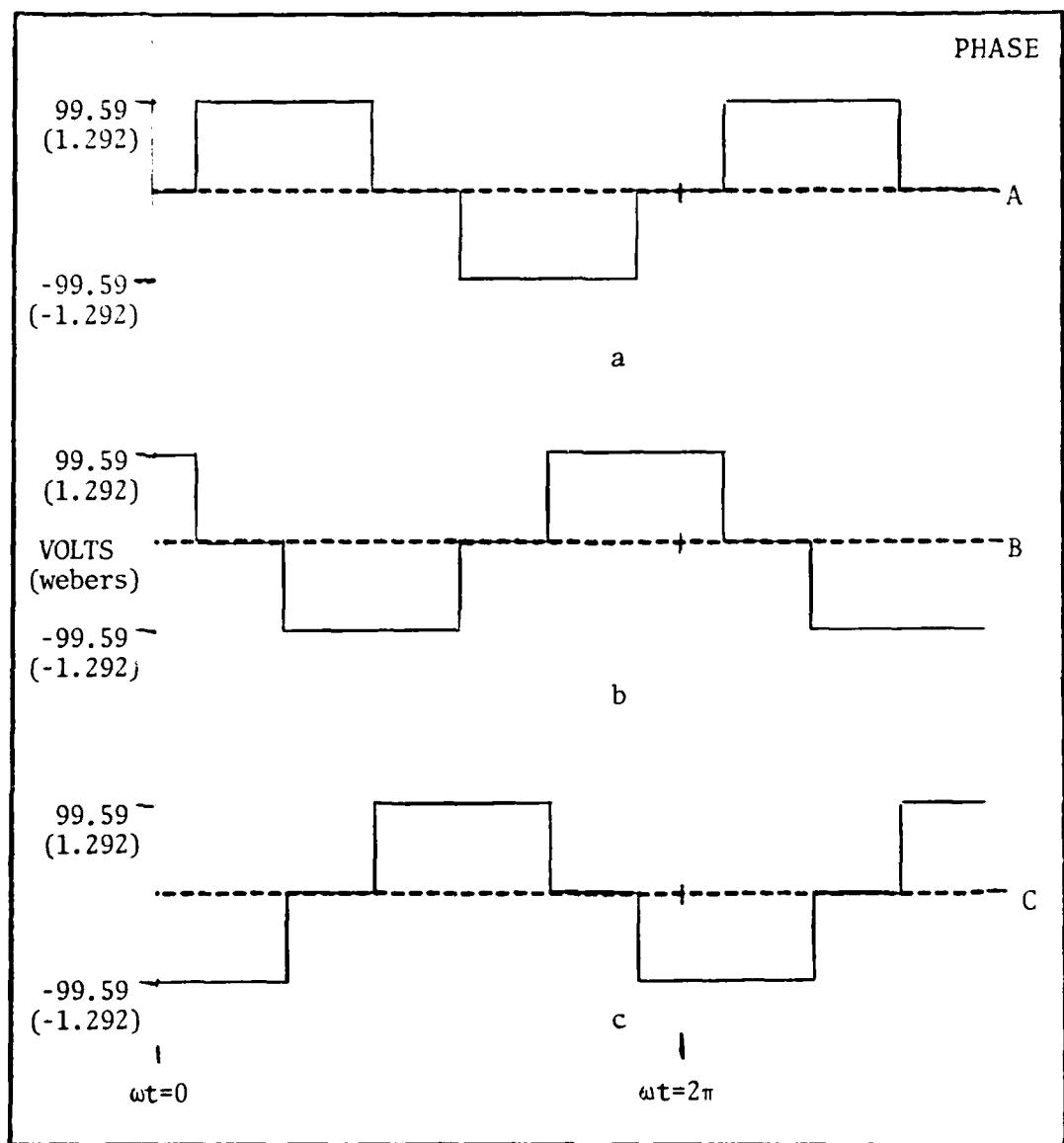


Figure 5 Time Variation of the Chosen Internal Phase Voltage and Flux Density

$$B = \frac{4}{\pi} \sum_{g=1}^{\infty} B_{\max} \frac{1}{g} \cos(g\pi/6) \sin(g\omega t) \quad (13)$$

where

$\omega$  is the frequency in radians/second

$g$  is the time harmonic number being considered

### Current

The phase current versus time is determined by the shape of the phase voltage waveform as well as the circuit impedances. Between current commutation periods, the phase current is the specified load voltage divided by the specified load impedance. The value of the phase current during commutation may be determined by the use of harmonic component analysis (Ref 12:400). Because the circuit may have frequency dependant impedances, each harmonic component of the current may have a different angle by which it lags the voltage of the same harmonic. The composite waveform accounts for the current lag. Another approach is to analyze the composite voltage waveform directly (Ref 7).

### Current Example

See Appendix I (Generator Design) for a reference on the generator specifications used in this example.

Because it is necessary to maintain the load power at 100 kilowatts, the DC load current is 125.51 amperes (100 kilowatts divided by  $460\sqrt{3}$  volts). There are no parallel

current paths inside the generator. Therefore, between commutation periods, the phase current is also 125.51 amperes.

Figure 6 shows the circuit of Figure 1 during a phase B to a phase A commutation. Phase C is conducting throughout this time, so no diodes are shown. It is assumed that the transmission line impedance and the generator resistance are negligible.

The phase voltage wave shape was given in Figure 5. A constant voltage ( $4 \cdot V_{coil}$ ) is applied across the inductive coils of phases A and B. The current in phase B linearly increases from zero and the current in A linearly decreases toward zero. The generator phase inductance for this example is chosen such that the current commutation angle is  $\pi/9$  electrical radians or equivalently 20 electrical degrees.

The current wave shape of the three phases is given in Figure 7. Notice how they follow the voltages of Figure 5. The time variation of the current for the three phases at selected times is given in Table 1.

The harmonic components of the phase current are:

$$I(t) = \sum_{g=1}^{\infty} \left( 36 I_{\max} / g \pi^2 \right) \left\{ \frac{\pi}{9} [\cos(g\pi/9) - \cos(g2\pi/9)] + \frac{1}{g} [\sin(g2\pi/9) - \sin(g\pi/9)] \right\} \sin g(\omega t - \pi/18) \quad (14)$$

where

$I(t)$  is the phase current in amperes

$I_{\max}$  is the maximum value of the phase current

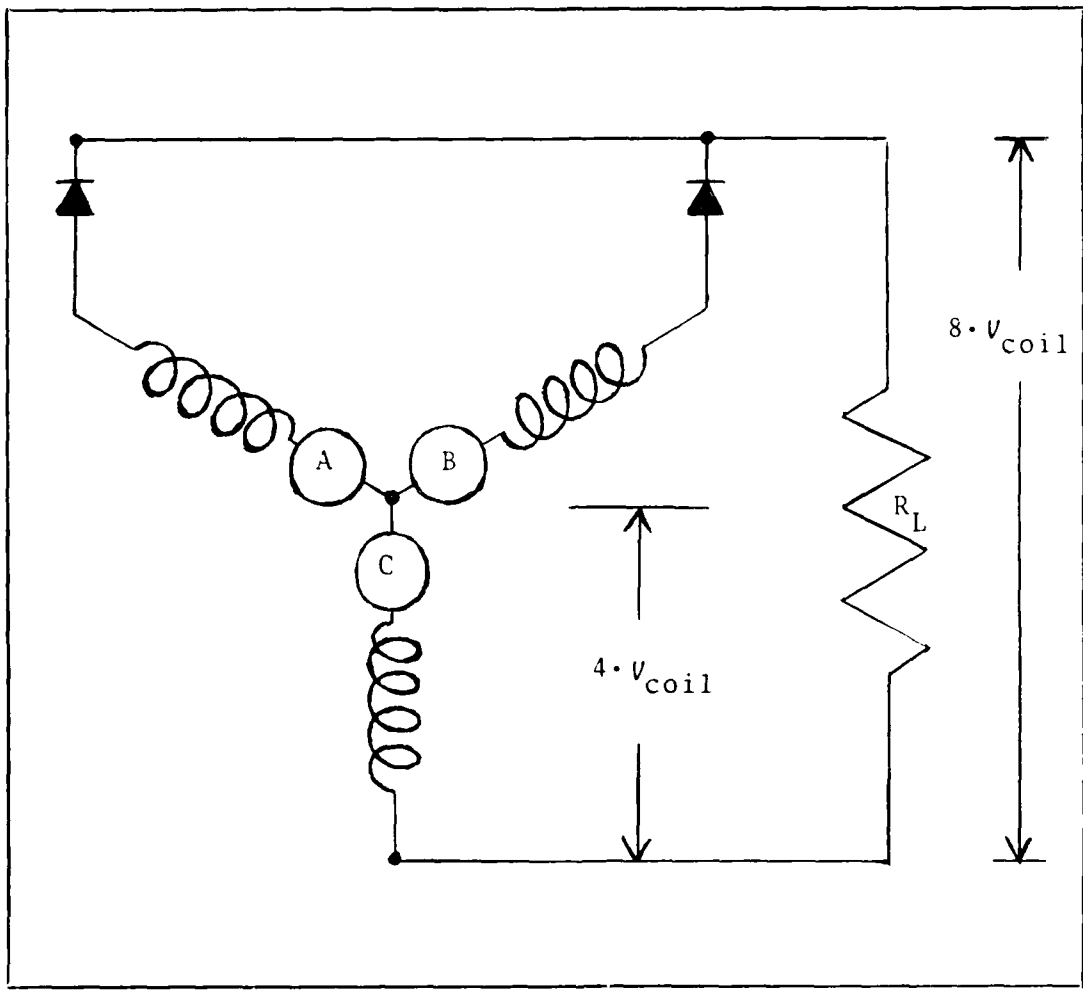


Figure 6 Equivalent Circuit During Commutation

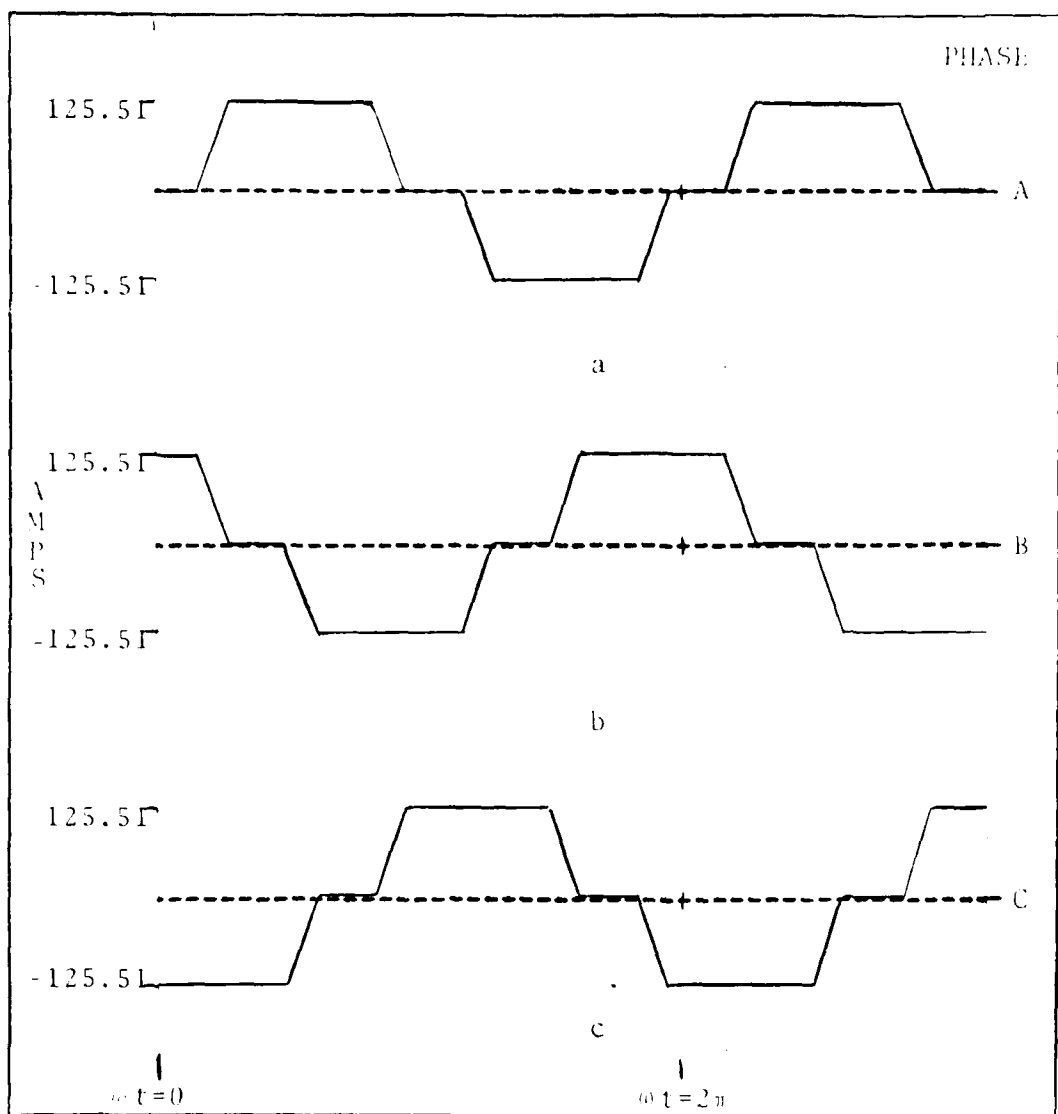


Figure 7 Time Variation of the Chosen Phase Current

Table 1 Normalized Current in Six Internal  
Phases versus Time

TIME ( $\omega t$ )	PHASE					
	A	B	C	A'	B'	C'
- $5\pi/15$	-1	1	0	1	-1	0
- $4\pi/15$	-1	1	0	1	-1	0
- $3\pi/15$	-1	1	0	1	-1	0
- $2\pi/15$	-.7	1	-.3	.7	-1	.3
$-\pi/15$	-.1	1	-.9	.1	-1	.9
0	0	1	-1	0	-1	1
$\pi/15$	0	1	-1	0	-1	1
$2\pi/15$	0	1	-1	0	-1	1
$3\pi/15$	.3	.7	-1	-.3	-.7	1
$4\pi/15$	.9	.1	-1	-.9	-.1	1
$5\pi/15$	1	0	-1	-1	0	1
$6\pi/15$	1	0	-1	-1	0	1
$7\pi/15$	1	0	-1	-1	0	1
$8\pi/15$	1	-.3	-.7	-1	.3	.7
$9\pi/15$	1	-.9	-.1	-1	.9	.1
$10\pi/15$	1	-1	0	-1	1	0

#### IV. Armature Reaction

This section develops an expression for the time variation of the MMF at each of the stator slots due to armature reaction.

As magnetic lines of flux inside a generator cut armature coils, a voltage is induced at the armature terminals. When a load is connected to the generator, current will flow through the armature coils generating an MMF known as armature reaction. Armature reaction MMF opposes the MMF due to the rotor field.

When the MMF from the rotor coils is added to the armature reaction MMF, the total MMF is found. The desired magnetic flux density can be produced provided that the correct air gap reluctance is present.

#### Single-Phase Winding

A single coil from each pole of a single-phase winding produces a square MMF wave around the air gap circumference. If the coils span the full width of a pole ( $T_p$ ), each coil has a width of  $\pi$  electrical radians. The magnitude of the MMF wave will oscillate with the frequency of the current in the coils.

The MMF under the armature coils may be expressed as the product of the time variation of the coil current and the Fourier components of the space variation of the square

MMF envelope. If the x coordinate (the distance along the circumference of the inside of the stator) is zero at a position which corresponds to the center of one of the full pitch coils, the space variation of the MMF per conductor is given by:

$$\text{MMF (for one conductor)} = I_{\max} \frac{2}{\pi} \sum_{v=1}^{\infty} \frac{1}{v} \sin(v\pi/2) \cos(v\pi x/\tau_p) \quad (15)$$

Because of the term  $\sin(v\pi/2)$ , the spacial variation has only odd harmonics. Because of the symmetry,  $\text{MMF}(-x) = \text{MMF}(x)$ , the coefficient of the  $\sin(v\pi x/\tau_p)$  terms in Equation (15) are all zero (and not shown).

The current in the coils is the phase current as described in Section III.

$$I(t) = I_{\max} \sum_{g=1}^{\infty} (a_g \sin g\omega t + b_g \cos g\omega t) \quad (16)$$

where

$a_g$  are the coefficients of the sine current harmonics

$b_g$  are the coefficients of the cosine current harmonics

Because:  $a \sin(\omega t + \phi) + b \cos(\omega t + \phi) = a' \sin \omega t + b' \cos \omega t$   
 a proper set of coefficients  $a_g$  and  $b_g$  may be established that account for the current lag angle of each harmonic. If, as is usually the case, the negative portion of the periodic current wave is a mirror image of the positive position, only odd harmonics exist in the time variation of the current.

A generator phase may contain several conductors distributed over one pole pitch in a single coil group. Since the current in each conductor is identical, the resultant MMF may be summed using the distribution factor  $K_{dv}$ . The space variation then becomes:

$$MMF(x) = MMF_{max} \frac{2}{\pi} \sum_{v=1}^{\infty} \frac{1}{v} \sin(v\pi/2) K_{dv} \cos(v\pi x/\tau_p) \quad (17)$$

where

$MMF_{max}$  is the maximum value of the MMF

$$MMF_{max} = qsI_{max} \quad (18)$$

where

$s$  is the number of turns of a coil group in a single stator slot

Notice that the coordinate  $x$  is now taken to be zero in the center of a coil group.

The space and time variation of a single phase is the product of the individual variations.

$$MMF(x, t) = MMF_{max} \left\{ \sum_{g=1}^{\infty} [a_g \sin(g\omega t) + b_g \cos(g\omega t)] \right\} \cdot \frac{2}{\pi} \sum_{v=1}^{\infty} \frac{1}{v} \sin(v\pi/2) K_{dv} \cos(v\pi x/\tau_p) \quad (19)$$

where

• indicates a product

$g$  is the time harmonic number being considered

### Distribution Example

See Appendix I (Generator Design) for a reference on the generator specifications used in this example.

The distribution factor for this example is:

$$\frac{\sin(v\pi/m)}{q \sin(v\pi/mq)} = \frac{\sin(v\pi/6)}{5 \sin(v\pi/30)} \quad (20)$$

### Polyphase Windings

If there is more than one coil group above each pole, the phase of each coil group must be considered in calculating the resultant MMF. The current in each coil group is dependent upon the connection of the internal machine phases to the load. If there are  $m$  internal phases, there will be  $m$  possible different time variations of current in the stator. Each current wave shape will be equally distributed in time with a separation angle of  $2\pi/m$  electrical radians.

As the current reaches maximum in successive phases, the maximum fundamental MMF occurs at the center of the successive coil groups. Successive coil groups correspond to successive internal machine phases. The MMFs are therefore distributed  $2\pi/m$  electrical radians apart.

The MMF due to all of the phases combined is the maximum MMF times the product of the time  $K(t,r)$  and space  $K(x,r)$  variations for all of the  $m$  internal phases.

$$K(t,r) = \sum_{g=1}^{\infty} [a_g \sin g(\omega t + r2\pi/m) + b_g \cos g(\omega t + r2\pi/m)] \quad (21)$$

where

$K(t, r)$  is the time MMF variation

$r$  is the individual internal machine phase

$$K(x, r) = \frac{2}{\pi} \sum_{v=1}^{\infty} \left[ \frac{1}{v} \sin(v\pi/2) K_{dv} \cos v(\frac{\pi x}{T_p} + r2\pi/m) \right] \quad (22)$$

where

$K(x, r)$  is the space MMF variation

$$\text{MMF}(x, t) = \text{MMF}_{\max} \sum_{r=0}^{m-1} [K(t, r) \cdot K(x, r)] \quad (23)$$

### Example

See Appendix I (Generator Design) for a reference on the generator specifications used in this example.

The space variation term in Equation (22) converges as it is summed over the integer  $v$  from one to infinity. The resulting value of the expression for the six internal phases ( $r = 0$  to  $r = 5$ ) and for the position of the five slots in phase C (Figure 2) is given in Table 2.

Table 2 Normalized Spacial Component of Armature Reaction,  $K(x, r)$ , at Slots of Phase C (Figure 2)

Phase	A	B	C	A'	B'	C'
x \ r	0	1	2	3	4	5
$\pi/30$	.5	.5	-.4	-.5	-.5	.4
$3\pi/30$	.5	.5	-.2	-.5	-.5	.2
$5\pi/30$	.5	.5	0	-.5	-.5	0
$7\pi/30$	.5	.5	.2	-.5	-.5	-.2
$9\pi/30$	.5	.5	.4	-.5	-.5	-.4

With the current wave shape that was established in Section III, it is possible to evaluate the armature reaction MMF at each of the slots versus time. According to Equation (23) and using data from Table 1 and Table 2, the products of the time variation and the space variation may be summed over the applicable phases. The number of internal phases,  $m$ , is equal to six in this example.

Notice that both the time and the space variation terms for phase A' are opposite in sign from the entries for phase A. The product of the space and time variation terms leads to a magnetic field from A' which is equal to the magnetic field from A both in magnitude and sign. Likewise the phases B and B' and the phases C and C' produce similar results. From Figure 2, a positive current in phase B produces an MMF under the slots of phase C which is opposite in direction to the MMF produced by a positive current in phase A.

The entries in Table 3 (Total Normalized Armature Reaction MMF) were obtained by changing the sign of the phase B and B' currents in Table 1 and by multiplying the resultant Table 1 array by the transpose of the array in Table 2. This multiplication is the direct normalized interpretation of Equation (23). In order to express the actual MMF, the entries must be multiplied by both the total number of conductors in series per internal machine phase and by the current which each conductor carries. Put another way, the entries in Table 3 multiplied by  $MMF_{max}$  (Equation 18) will yield the actual MMF.

Table 3 Normalized Total Armature Reaction  
MMF at slots of Phase C

TIME ( $\omega t$ ) \ X	$\pi/30$	$3\pi/30$	$5\pi/30$	$7\pi/30$	$9\pi/30$
$-5\pi/15$	-2.00	-2.00	-2.00	-2.00	-2.00
$-4\pi/15$	-2.00	-2.00	-2.00	-2.00	-2.00
$-3\pi/15$	-2.00	-2.00	-2.00	-2.00	-2.00
$-2\pi/15$	-1.46	-1.58	-1.70	-1.82	-1.94
$-\pi/15$	.38	.74	1.10	1.46	1.82
0	.20	.60	1.00	1.40	1.80
$\pi/15$	.20	.60	1.00	1.40	1.80
$2\pi/15$	.20	.60	1.00	1.40	1.80
$3\pi/15$	.40	0	.40	.80	1.20
$4\pi/15$	1.60	1.20	.80	.40	0
$5\pi/15$	1.80	1.40	1.00	.60	.20
$6\pi/15$	1.80	1.40	1.00	.60	.20
$7\pi/15$	1.80	1.40	1.00	.60	.20
$8\pi/15$	1.86	1.58	1.30	1.02	.74
$9\pi/15$	1.98	1.94	1.90	1.85	1.82
$10\pi/15$	2.00	2.00	2.00	2.00	2.00

## V. Rotor MMF

This section develops an expression for the MMF due to the rotor coils.

The rotor coils are a significant source of MMF in the generator. Therefore, the affect on the controlled magnetic circuit must be accounted for.

Two different effects from the rotor are to be investigated in the search for a solution to the problem of harmonic control. In Section VII, the approach is to use the rotating rotor field MMF (rotating with respect to the stator) to cancel certain rotating MMF (again rotating with respect to the stator) components created by the armature reaction. This procedure requires a properly designed MMF over the rotor surface.

In contrast, Section VIII and Section IX capitalize on the reluctance of the rotor for control. For this case, the assumption is made that most of the MMF drop is across the air gap reluctance and that the rotor MMF may be represented (first order) as a square wave over the rotor surface. With these assumptions, the development of the rotor MMF expression and its translation into stator coordinates is continued.

Without fringing, the width of each square MMF pulse is equal to the rotor pole arc  $b_p$ . Therefore, the pitch factor  $K_{pv}$ , may be used to form the MMF expression.

$$\text{MMF}_{\text{rotor}} = \frac{4}{\pi} s_r I_F \sum_{v=1}^{\infty} \frac{1}{v} \sin(v\pi b_p/2T_p) \cos(v\pi x'/T_p) \quad (24)$$

where

$\text{MMF}_{\text{rotor}}$  is the rotor MMF in ampere turns

$s_r$  is the number of turns in a rotor coil

$I_F$  is the rotor current in amperes

$b_p$  is the rotor pole arc in radians or slots

$x'$  is the distance along the outside circumference of the rotor in meters (rotor coordinates)

The zero (origin) of the rotor coordinate system is taken at a pole center.

The MMF expression for non-constant MMF across the pole face may also be achieved by Fourier analysis. In this case, saturation and fringing are the means of achieving the desired effect. Finite Element analysis (Section X) is an important tool to use when considering saturation and fringing.

Each harmonic component of the rotor MMF travels with respect to the stator and has the same velocity as the rotor. The MMF due to the rotor can be transformed into the stator's set of polar coordinates by transforming each harmonic component into a forward traveling wave.

$$\text{MMF}_{\text{rotor}} = \frac{4}{\pi} s_r I_F \sum_{v=1}^{\infty} \frac{1}{v} \sin(v\pi b_p/2T_p) \cos[(v\pi x/T_p) - v\omega t] \quad (25)$$

The MMF which drives a flux tube may be moved around that tube without changing the flux density. Therefore with radial flux lines, the traveling square wave can be projected across the air gap with the same angular coordinates.

As was true of the armature MMF expression, the rotor MMF versus time can be evaluated at any  $x$  by substitution of that value. Rotor MMF is opposed by the armature reaction MMF. The MMFs may be algebraically summed to obtain an expression for the total MMF along the stator (Section VI).

#### Example

See Appendix I (Generator Design) for a reference on the generator specifications used in this example.

The chosen pole arc is  $2\pi/3$  electrical radians. There are 533 ampere turns in each rotor winding. The rotor MMF is a square wave which travels with the rotor under the armature coils. The time variation of the rotor MMF under the slots of phase C (Figure 2) is given in Table 4.

Table 4 Rotor MMF

TIME ( $\omega t$ )	x	$\pi/30$	$3\pi/30$	$5\pi/30$	$7\pi/30$	$9\pi/30$
$-5\pi/15$		0	0	0	0	0
$-4\pi/15$		533	0	0	0	0
$-3\pi/15$		533	533	0	0	0
$-2\pi/15$		533	533	533	0	0
$-\pi/15$		533	533	533	533	0
0		533	533	533	533	533
$\pi/15$		533	533	533	533	533
$2\pi/15$		533	533	533	533	533
$3\pi/15$		533	533	533	533	533
$4\pi/15$		533	533	533	533	533
$5\pi/15$		533	533	533	533	533
$6\pi/15$		0	533	533	533	533
$7\pi/15$		0	0	533	533	533
$8\pi/15$		0	0	0	533	533
$9\pi/15$		0	0	0	0	533
$10\pi/15$		0	0	0	0	0

## VI. Total MMF

Section IV developed an expression for the armature reaction MMF and Section V developed an expression for the rotor MMF. These MMFs are superimposed in the generator's air gap. Each MMF produces a magnetic flux density with space and time variations that are superimposed. This section develops an expression for the total MMF.

At first glance it seems possible to calculate the flux density due to armature reaction and then to adjust the rotor reluctance so the rotor MMF produces a cancelling flux density. This idea is flawed because a change in the magnetic circuit also changes the magnetic flux density driven by the armature reaction MMF. Therefore, instead of the superposition of flux density, it is the superposition of the MMF which must be accomplished. The desired flux density may then be obtained from the total MMF by adjusting the air gap reluctance.

The total MMF in the generator is the sum of the expressions in Equation (23) and Equation (25). Because of the direction defined for positive current (Figure 2), the armature reaction MMF and the rotor MMF add.

As is shown in Section VII, specification of rotor MMF is not sufficient to control the generator MMF for all of the air gap for all times. The armature reaction MMF produces both space and time variations that are not controlled by the

rotor MMF. Substitution of the space or the time into the expressions however, brings the terms of both the armature reaction MMF and the rotor MMF to a countably infinite series. The coordinates of the stator conductors are important since it is at these points that the time variation of the flux density creates the desired voltage wave shape. With this substitution, control of the harmonics is approached in Section VIII and Section IX.

Example

See Appendix I (Generator Design) for a reference on the generator specifications used in this example.

The actual armature reaction MMF is obtained by multiplying the normalized armature reaction MMF in Section IV by  $\text{MMF}_{\max}$  (Equation 18). The total MMF can be obtained by summing the armature reaction MMF and the rotor MMF. This is equivalent to multiplying Table 3 by  $\text{MMF}_{\max}$  and adding the result to Table 4. The total MMF is shown in Table 5.

Table 5 Total MMF at Phase C Slots versus Time

TIME $(\omega t)$	$\pi/30$	$3\pi/30$	$5\pi/30$	$7\pi/30$	$9\pi/30$
$-5\pi/15$	-1255.1	-1255.1	-1255.1	-1255.1	-1255.1
$-4\pi/15$	-722.1	-1255.1	-1255.1	-1255.1	-1255.1
$-3\pi/15$	-722.1	-722.1	-1255.1	-1255.1	-1255.1
$-2\pi/15$	-383.2	-458.5	-533.8	-1142.1	-1217.4
$-\pi/15$	294.5	68.6	-157.3	-333.2	-1142.1
0	407.5	156.5	-94.6	-345.6	-596.6
$\pi/15$	407.5	156.5	-94.6	-345.6	-596.6
$2\pi/15$	407.5	156.5	-94.6	-345.6	-596.6
$3\pi/15$	784.0	533.0	282.0	31.0	-220.0
$4\pi/15$	1537.1	1286.1	1035.0	784.0	533.0
$5\pi/15$	1662.6	1411.6	1160.6	909.5	658.5
$6\pi/15$	1129.6	1411.6	1160.6	909.5	658.5
$7\pi/15$	1129.6	878.6	1160.6	909.5	658.5
$8\pi/15$	1167.2	991.5	815.8	1173.1	997.4
$9\pi/15$	1242.5	1217.4	1192.3	1167.2	1675.1
$10\pi/15$	1255.1	1255.1	1255.1	1255.1	1255.1

## VII. MMF Cancellation

This section considers rotor MMF for the cancellation of selected armature reaction MMF harmonic components. For this analysis, it is useful to express both the armature reaction MMF and the rotor MMF as traveling waves.

### Armature Reaction MMF

Equation (23) is the expression for the armature reaction MMF. Symmetry about the time origin causes the cosine terms in  $K(t,r)$  (Equation 21) to be zero. The cosine term due to asymmetry is subsequently considered. For a given  $g$  and  $v$ , several constants from Equation (23) may be combined by letting:

$$A_{gv} = \frac{2}{\pi} q_s I_{max} a_g \sin(v\pi/2) K_{dv}/v \quad (26)$$

where

$A_{gv}$  is a constant whose value depends on  $g$  and  $v$

Remembering that the cosine coefficient in Equation (21) is zero, the armature reaction MMF expression from Equation (23) can be rewritten as:

$$\text{MMF}(x,t) = \sum_{g=1}^{\infty} \sum_{v=1}^{\infty} \sum_{r=0}^{m-1} A_{gv} \sin g(\omega t + r2\pi/m) \cdot \cos v[(\pi x/T_p) + (r2\pi/m)] \quad (27)$$

Using the trigonometric identity

$$\sin(\alpha) \cos(\beta) = \frac{1}{2} \sin(\alpha - \beta) + \frac{1}{2} \sin(\alpha + \beta) \quad (28)$$

Equation (27) may be rewritten as:

$$\begin{aligned}
 \text{MMF}(x, t) &= \sum_{g=1}^{\infty} \sum_{v=1}^{\infty} \frac{1}{2} A_{gv} \cdot \\
 &\left\{ \sin [(g\omega t) + v\pi x/T_p] + \sin [(g\omega t) - (v\pi x/T_p)] \right. \\
 &+ \sin [(g\omega t) + (v\pi x/T_p) - (g+v)\frac{2\pi}{m}] + \sin [(g\omega t) - (v\pi x/T_p) - (g-v)\frac{2\pi}{m}] \\
 &+ \sin [(g\omega t) + (v\pi x/T_p) - (g+v)\frac{4\pi}{m}] + \sin [(g\omega t) - (v\pi x/T_p) - (g-v)\frac{4\pi}{m}] \\
 &\quad \vdots \quad \vdots \\
 &+ \sin [(g\omega t) + (v\pi x/T_p) - (g+v)\frac{(m-1)2\pi}{m}] + \sin [(g\omega t) - (v\pi x/T_p) - (g-v)\frac{(m-1)2\pi}{m}] \left. \right\} \\
 &\quad (29)
 \end{aligned}$$

Equation (29) contains the positive direction (terms in the right column of the equation) and negative direction (terms in the left column of the equation) traveling waves.

When  $\psi$  is a multiple of  $m$ ,

$$\sin \theta + \sin(\theta + \psi \frac{2\pi}{m}) + \sin(\theta + \psi \frac{4\pi}{m}) + \dots + \sin(\theta + \psi \frac{(m-1)2\pi}{m}) = m \sin C \quad (30a)$$

When  $\psi$  is not a multiple of  $m$ ,

$$\sin \theta + \sin (\theta + \psi \frac{2\pi}{m}) + \sin (\theta + \psi \frac{4\pi}{m}) + \dots + \sin (\theta + \psi \frac{(m-1)2\pi}{m}) = 0 \quad (30b)$$

This also holds true for a cosine sum with equivalent arguments.

Because the use of sines and cosines in  $K(t,r)$  preserves symmetry about the origin,  $g$  and  $v$  are both odd integers. Therefore, their sums and differences must be even.

With  $\psi$  analogous to  $(g + v)$  or  $(g - v)$  in Equations (30a) and (30b)

$$\text{MMF}(x, t) = \sum_{g=1}^{\infty} \sum_{v=1}^{\infty} \left[ \frac{m}{2} A_{gv} \sin(g\omega t + \frac{v\pi x}{T_p}) + \frac{m}{2} A_{gv} \sin(g\omega t - \frac{v\pi x}{T_p}) \right] \quad (31)$$

where for the first sine term  $(g+v)$  is an even multiple of  $m$  and for the second sine term  $(g-v)$  is an even multiple of  $m$ .

When the cosine term in  $K(t, r)$  is not zero, the traveling waves may also be found. When

$$B_{gv} = \frac{2}{\pi} q_s I_{\max} b_g \sin(v\pi/2) K_{dv}/v \quad (32)$$

where

$B_{gv}$  is a constant whose value depends on  $g$  and  $v$

the cosine term in Equation (21) leads to:

$$\text{MMF}(x, t) = \sum_{g=1}^{\infty} \sum_{v=1}^{\infty} \sum_{r=0}^{m-1} B_{gv} \cos g(\omega t + r2\pi/m) \cos v[(\pi x/T_p) + (r2\pi/m)] \quad (33)$$

The trigonometric identity

$$\cos(\alpha) \cos(\beta) = \frac{1}{2} \cos(\alpha+\beta) + \frac{1}{2} \cos(\alpha-\beta) \quad (34)$$

yields:

$$\text{MMF}(x, t) = \sum_{g=1}^{\infty} \sum_{v=1}^{\infty} \left[ \frac{m}{2} B_{gv} \cos(g\omega t + \frac{v\pi x}{T_p}) + \frac{m}{2} B_{gv} \cos(g\omega t - \frac{v\pi x}{T_p}) \right] \quad (35)$$

where for the first cosine term  $(g+v)$  is an even multiple of  $m$  and for the second cosine term  $(g-v)$  is an even multiple of  $m$ .

Therefore, the complete expression for the time variation of the magnetic field (armature reaction MMF only) referenced to a fixed stator due to the specified  $m^{\text{th}}$  internal phase armature current is:

$$\begin{aligned} \text{MMF}(x, t) = \sum_{g=1}^{\infty} \sum_{v=1}^{\infty} & \left[ \frac{m}{2} A_{gv} \sin(g\omega t + v\frac{\pi x}{T}) + \frac{m}{2} B_{gv} \cos(g\omega t + v\frac{\pi x}{T}) \right. \\ & \left. + \frac{m}{2} A_{gv} \sin(g\omega t - v\frac{\pi x}{T}) - \frac{m}{2} B_{gv} \cos(g\omega t - v\frac{\pi x}{T}) \right] \end{aligned} \quad (36)$$

As before, for the first two terms,  $(g+v)$  is an even multiple of  $m$  and for the last two terms,  $(g-v)$  is an even multiple of  $m$ .

### Example

See Appendix I (Generator Design) for a reference on the generator specifications used in this example.

For  $m=6$ , the terms of Equation (36) are non-zero when  $(g+v)$  or  $(g-v)$  is a multiple of 6. Therefore,

$$v = \pm 6k - g \quad (37)$$

where

$k$  is an integer constant equaling 0,  $\pm 1$ ,  $\pm 2$ , ...

Table 6 gives the space harmonic indexes (values of  $v$ ) corresponding to the odd harmonics of the time variation of the armature reaction MMF. A forward traveling wave is

represented by  $\sin(g\omega t - v \frac{\pi x}{T_p})$ . The velocity of the traveling wave components relative to that of the rotor is equal to the negative time harmonic index (-g) divided by the space harmonic index (v).

Table 6 Space Harmonic Indexes for Armature Reaction Traveling Waves

$g \backslash k$	0	-1	+1	-2	+2	-3	+3
1	-1	5	-7	11	-13	17	-19
3	-3	3	-9	9	-15	15	-21
5	-5	1	-11	7	-17	13	-23
7	-7	-1	-13	5	-19	11	-25
9	-9	-3	-15	3	-21	9	-27
11	-11	-5	-17	1	-23	7	-29
13	-13	-7	-19	-1	-25	5	-31
15	-15	-9	-21	-3	-27	3	-33
17	-17	-11	-23	-5	-29	1	-35

### Comparison

The traveling wave for the rotor MMF is expressed in Equation (25). The harmonic index (v) in each component is the same for the time and space variation.

The cancellation of two orthogonal functions (Ref 10:188)

$$A \sin(\alpha t) + B \sin(\beta t) = 0 \quad (38)$$

requires that the magnitudes of  $\alpha$  and  $\beta$  are equal or that both A and B are zero. This applies to the cancellation of armature reaction MMF terms (Equation 36) and rotor MMF terms Equation (25).

If cancellation is to apply to all positions ( $x$ ) and all times ( $t$ ), the rotor MMF can only be used in cancellation of armature reaction MMF terms in which  $g=v$ . In other words, rotor MMF will only cancel armature reaction MMF that has the same relative velocity ( $g/v$ ); the velocity of the rotor.

Specification of rotor MMF is not sufficient to control the generator MMF for all of the air gap at all times. The armature reaction MMF produces both space and time variations that are not cancelled. This limited cancellation is more effectively accomplished by the specification of other parameters such as pole arc (see Section II).

Another concern with this approach is that the reluctance function controls the flux density according to Equation (7). Thus, even if a certain MMF harmonic is cancelled, there must be protection from the reintroduction of that harmonic through the variation of the reluctance. Therefore, the use of rotor MMF is not a favored approach in the control of generator harmonics.

## VIII. Reluctance Harmonic Control

This section describes an attempt to control phase voltage harmonics by using the reluctance to control the flux density harmonics.

Neglecting saturation and considering the air gap to be dominant, the reluctance along the air gap is proportional to the air gap distance. In addition, because the air gap rotates with the rotor, the reluctance versus distance has the same shape as the reluctance versus time at a fixed point on the stator. Therefore, although the reluctance requirements may be solved on a time basis, it can be directly related back to the air gap and thus rotor geometry. MMF( $x, t$ ) and MMF( $t$ ) refer in this section to total MMF.

### Flux Density from MMF

Just as it is the combined voltage of all the conductors connected in series in a coil group which is specified as phase voltage, it is the sum of the flux densities cutting these same conductors that must be controlled. The flux density at each stator slot is determined by the MMF available to force the flux through the reluctance at that point.

The MMF( $x, t$ ) around the stator is known. It is the superposition of the MMF( $x, t$ ) due to the armature reaction MMF (Section IV) and the MMF<sub>rotor</sub> due to the rotor coils (Section V). The time variation MMF( $t$ ) at any location along the stator may be obtained by substituting that location's

coordinates into the  $\text{MMF}(x,t)$  expression. For a given  $\text{MMF}(t)$ , the value of reluctance determines the magnetic flux density. Therefore, for a given  $\text{MMF}(x,t)$ , the desired phase voltage (Section III) may be had by controlling the reluctance.

The reluctance at any location along the stator periphery is also a function of time. Therefore, the total magnetic flux density is:

$$B_{\text{TOT}} = \sum_{x=1}^q B_x(t) = \sum_{x=1}^q \frac{\text{MMF}_x(t)}{R_x(t) \cdot \text{Area}} \quad (39)$$

where

$\text{Area}$  is the rotor surface area under a single coil group

$B_{\text{TOT}}$  is the total magnetic flux density

$B_x(t)$  is the magnetic flux density at slot  $x$

$\text{MMF}_x(t)$  is the MMF at slot  $x$

$R_x(t)$  is the reluctance at slot  $x$

If, during certain periods  $T_v$ , the air gap distance under a slot is proportional to the MMF,

$$\left. \delta(t) \right|_{T_v} = K \cdot \text{MMF} \quad (40)$$

where

$K$  is a proportionality constant

then the flux density, Equation (8), is a constant over that period.

$$B = \mu/K \quad (41)$$

If the value of the proportionality constant K is changed, the magnitude of the flux density is also changed. The basis for this concept involves a series of these changes combined with careful control of the flux density harmonics.

#### Reluctance Specification Concept

The magnetic circuit reluctance function is periodic. The reluctance at any slot is the same function as the reluctance at a previous slot except for a time delay. If the MMF(t) expression for each slot is shifted instead, the sum on the right side of Equation (39) has a common denominator. Using the shifted and summed MMF<sup>\*</sup>(t) reflected into the first slot, the solution of reluctance versus time will be simplified.

A pulse width current modulation technique for control of line voltage harmonics was presented by Krishnamurthy (Ref 11:1269). His technique is reinterpreted for the time variation of the magnetic circuit. Here permeance is modulated to control the magnetic field.

The resulting flux density variation B(t) will consist of a set of symmetrically shaped increments for each set of harmonic(s) controlled (see Figure 8c). The set of increment centers for the n<sup>th</sup> controlled harmonic is given the name C<sub>n</sub> (see Figure 8b) which corresponds to B<sub>n</sub> in Reference 11.

$$B_v(C_n + \Delta t) = B_v(C_n - \Delta t) \quad (42)$$

and

$$B_v(2k\pi + C_n) = -B_v(2k\pi - C_n) = B_v[(2k+1)\pi - C_n] = -B_v[(2k+1)\pi + C_n] \quad (43)$$

where

$k$  is an integer constant equaling 0, +1, +2, ...

The product of the permeance and the MMF will be constant in magnitude over the increments, but will change sign every  $\pi$  radians.

The coefficient of the  $n^{\text{th}}$  harmonic of the flux density is

$$b_v = \frac{8}{v\pi} \frac{B_{\max}}{d} \sin v d \sum_{n=1}^c \sin vC_n \quad (44)$$

where

$d$  is the width of an increment (maximum  $\Delta t$ )

$c$  is the number of harmonics controlled by the increments of concern

When the  $C_n$ 's are chosen such that:

$$\sum_{n=1}^c \sin vC_n = 0 \quad (45)$$

$b_v$  can be made equal to zero for  $c$  different harmonics. There will be  $4c$  pulses per  $2\pi$  electrical radians.

### Methodology

The harmonics of the flux density are controlled by respecification of the air gap length under the stator slots during certain periods  $T_n$ . The  $T_n$  periods correspond to the non-zero periods of the modulated wave calculated for no disturbance of the  $n$  previously controlled harmonics. The air gap length over each period is such that although there is variation in the MMF, the flux density is constant. The process is accomplished one harmonic at a time with the fundamental completed last.

For the first non-fundamental harmonic to be controlled,  $v_1$ , the periods  $T_o$  correspond to the entire pole arc.

Equation (8) is rearranged to solve for the length of the air gap over the desired periods.

$$\delta(t) = \frac{\mu_{\text{air}} \text{MMF}(t) R}{B_v} \quad (46)$$

The desired values for the flux density are given by rearrangement of Equation (10).

$$B_v = \frac{V_v}{v\ell} \quad (47)$$

For the second harmonic to be controlled,  $v_2$ , the air gap is respecified over the periods  $T_1$ . The centers,  $c_{v_1}$ , of those periods are chosen in each fundamental frequency quarter cycle so that Equation (45) is satisfied ( $c=1$ ). Therefore, there will be no contribution to the  $v_1$  harmonic from the

respecification. The width of the periods is extended to the point that they meet each other or the edge of the rotor pole. The respecification (addition of an increment of permeance over the periods  $T_1$ ) is done so that the  $v_2$  time harmonics of the flux density are the proper value.

Equation (41) is used to calculate the flux density component for  $v_2$  above the pole arc outside of  $T_1$ . The remainder of the necessary flux density,  $\Delta B_{v_1}$ , must come from the period  $T_1$ . The flux density to be added over the periods  $T_1$  must be a constant according to the modulation technique.

Reluctance is proportional to  $\delta$ . If the needed reluctance is  $\delta'$  and the present reluctance is  $\delta$ , the reluctance to be added is the difference. Returning to the distance domain, the new air gap length must be  $\delta' \cdot \delta / (\delta - \delta')$ . The respecification for  $\Delta B_v$  becomes

$$\frac{\delta' \cdot \delta}{\delta - \delta'} = \frac{\mu}{\Delta B_v} \text{ MMF}(t)_R \quad (48)$$

If  $T_n$  extends over the boundaries of previous  $T$ , Equation (48) will be valid as long as the proper  $\delta$  versus time is used. Further harmonics are controlled by additional increments of reluctance.

#### Example

See Appendix I (Generator Design) for a reference on the generator specifications used in this example.

The third harmonic is chosen as the first to be controlled. The desired flux density is zero. From Equation (46),  $\delta$  is infinite.

$T_1$  is now determined for control of the fifth harmonic (the second to be controlled) without disturbance of the third harmonic. The sum

$$\sum_{n=1}^1 \sin v_n C_n$$

is zero for  $C_n = \pi/3$ . The centers,  $C_1$ ,  $\pi/3$  radians away from each multiple of  $\pi$  radians are  $\pi/3$ ,  $2\pi/3$ ,  $4\pi/3$ , and  $5\pi/3$ . The width of each increment may be up to  $\pi/3$  before they touch. At this full width, the outside limits of the increments  $T_1$  are  $\pi/6$  to  $5\pi/6$  and  $7\pi/6$  to  $11\pi/6$ . The merged increments are  $2\pi/3$  wide corresponding to the width of the chosen  $2\pi/3$  pole arc. In other words, a  $2\pi/3$  pole arc constant air gap produces no third harmonic. This is consistent with conventional pole arc design (Ref 9:34).

The desired flux density for the fifth harmonic comes from Section III and Equation (47). All of this flux must come from  $T_1$  because the rotor pole arc does not extend past  $T_1$ . From Equation (48) and the fact that  $\delta$  is infinite,  $\delta'$ , (the limit of  $[\delta' \cdot \delta / (\delta - \delta')]$  as  $\delta$  goes to infinity) may be found.

Next,  $T_2$  is determined for control of the next harmonic without disturbance of the third and fifth harmonics. Equation (45) is simultaneously solved for  $v=3$  and  $v=5$  yielding  $C_5 = .255^\circ$

and  $C_5 = .433\pi$ . The centers of the  $B_{v_2}(t)$  pulses are  $.253\pi$ ,  $.433\pi$ ,  $.566\pi$ ,  $.766\pi$ ,  $1.233\pi$ ,  $1.433\pi$ ,  $1.566\pi$ , and  $1.766\pi$  radians. The periods meet and extend to the edge of the pole when their width is  $.166\pi$  radians. The reluctance and flux density waves built with these periods are shown in Figures 8a and 8c. The air gap length over these periods is adjusted to provide the necessary flux density not provided outside of  $T_2$ . The flux density adjustment continues in this manner for other harmonics. The reluctance over the final periods  $T_n$  which affect none of the previously controlled harmonics is adjusted for the fundamental component.

A graphical interpretation helps clarify the process. The periods of non-infinite reluctance, shown in Figure 8b, are calculated as previously described. The air gap length (proportional to reluctance) is obtained during each period by Equation (46). The product of the MMF and the reluctance (the flux density variation) is shown in Figure 8c.

The components of the sine  $a_v^*$  and cosine  $b_v^*$  parts of the each harmonic of the flux density may be calculated from:

$$a_v^* = \frac{1}{\pi} \int_{-\pi}^{\pi} B \sin v\omega t dt \quad (49)$$

$$b_v^* = \frac{1}{\pi} \int_{-\pi}^{\pi} B \cos v\omega t dt \quad (50)$$

The curved bound of the shaded areas in Figure 8d and 8f represent the integrand of Equation (49) where  $v=5$  and  $5$

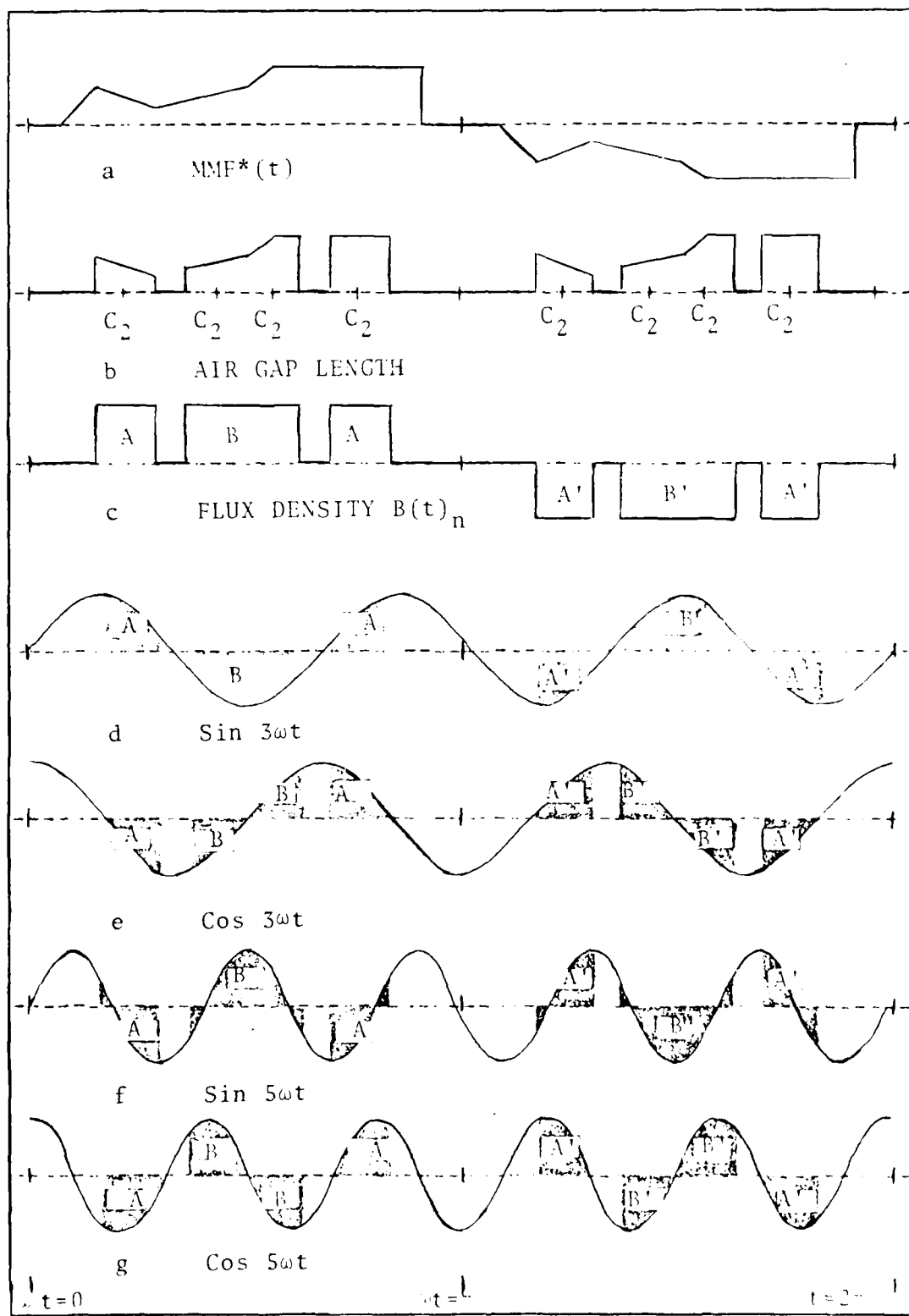


Figure 8 Reluctance Harmonic Control Example Wave Shapes

respectively. The curved bound of the shaded areas in Figures 8e and 8f represent the integrand of Equation (50) when  $v=3$  and 5 respectively.

The signed shaded areas in Figures 8d through 8g represent the integrals from Equations (49) and (50). Algebraically, the signed areas of Figures 8d through 8g sum to zero. This illustrates that Equations (49) and (50) are zero for  $v=3$  and for  $v=5$ . Thus, the harmonic components are zero for these harmonics because of the chosen reluctance values and periods. The illustration is similar for other higher harmonics.

#### How Many Harmonics

The process as described, approaches the desired flux density wave shape one harmonic at a time. To see the advantage of this approach, consider specification of the reluctance as a composite wave shape.

$$\delta(t) = \frac{\mu_{air} MMF(t)}{B(t)} \quad (51)$$

where

$\delta(t)$  is a time varying air gap

This requires a specific finite reluctance at all times. When the large air gap between the poles is under the coil group, the reluctance is not variable. This shortcoming affects all the harmonics. Therefore, the chosen method, because the important harmonics can be directly controlled has an advantage.

The number of harmonics which can be controlled is dependent on those chosen and the pole arc. Equation (45) yields  $C_1 = .183\pi$ ,  $C_2 = .344\pi$ , and  $C_3 = .433\pi$ , for control of the 3rd, 5th, and 7th harmonics. If the pole arc length was less than  $.633\pi$ ,  $C_3$  would be at the pole edge and control of these three harmonics could not be achieved. Therefore, the harmonics and the pole arc must be selected consistent with the methodology.

#### The Contradiction

The concept of harmonic control appears to be practical once  $\text{MMF}_R$  (the reflected MMF) is obtained and the control harmonics are selected. However, obtaining  $\text{MMF}_R$  is not an easy problem.

The proposed shift of MMF at consecutive slots 1 and 2 is

$$\text{MMF}_1^*(t) = \text{MMF}_2(t - \Delta t) \quad (52)$$

where

$\text{MMF}_1^*(t)$  is the shifted MMF

The reluctance at one slot is the same function as the reluctance at the previous slot except for a delay of  $\Delta t$ .

In other words

$$R_1(t) = R_2(t - \Delta t) \quad (53)$$

An expression for the flux density at the second slot is

$$B_2(t - \Delta t) = \frac{MMF_2(t - \Delta t)}{R_2(t - \Delta t)} \quad (54)$$

The shifted MMF and reluctance are then plugged into Equation (54). The contradiction is that the flux density  $B_2(t - \Delta t)$  reflected into the first slot is not synchronized with the flux density at the first slot  $B_1(t)$ . Such a sum makes little sense.

A general solution for a reflected  $B_2(t)$  synchronized with  $B_1(t)$  and with the knowledge of  $MMF_2(t)$ , but not  $R_2(t)$  exceeds the resources of this thesis effort. Therefore, another approach is preferred.

## IX. Incremental Reluctance Specification

This section describes the final method in which the rotor geometry specification is analyzed for control of the generated voltage wave shape. The reluctance of the air gap is specified as the traveling rotor is positioned under consecutive stator slots. Just as in Section VIII, reluctance versus time may also be related to air gap distance versus time and thus to rotor geometry. The specification progresses with time along with the required wave shape. Therefore, individual harmonic components are not of concern.

### MMF to Flux Density

The total MMF versus time which was developed in Section VII is a useful starting place for this development. The reluctance must be specified so that the resulting magnetic flux density will be in accordance with the magnetic flux density required, as was discussed in Section III. Air gap dominance, the lack of fringing, and the finite permeance effects are assumed here as they were in Section VIII.

The reluctance at any slots is the same function as the reluctance at the previous slot except for a time delay of  $\Delta t$ .

$$\Delta t = \frac{\alpha_e}{v_{ang}} \quad (55)$$

where

$v_{ang}$  is the rotor angular velocity

$\alpha_e$  is the electrical angle between slots

Therefore, the total flux density may be expressed as:

$$B_{TOT}(t) = \sum_{n=1}^q B_n(t) = \sum_{n=1}^q \frac{MMF_n(t)}{R_1(t-n\Delta t)} \quad (56)$$

where

n is the individual stator slot number

#### Reluctance Specification

When the gap between salient poles is under a slot, the reluctance at that slot may be approximated as infinite. When the rotor turns so that its edge is between the first and second conductor of the relevant coil group, Equation (56) has a non-zero term only for n=1. The desired increment of flux density,  $\Delta B$ , and the available MMF determine the reluctance required while the rotor edge is between slots 1 and 2.

$$R_1(t) = \frac{MMF_1(t)}{\Delta B(t)} \quad (57)$$

After a delay of  $t$ , that same reluctance will appear under the second slot. The  $MMF_2$  at  $(t+\Delta t)$  and the already specified reluctance will determine the flux density at the second slot. The remainder of the desired total flux density must come under the first slot. By using  $MMF(t+\Delta t)$  and the residual requirement of reluctance,  $\Delta B$ , in Equation (57), the reluctance at the next increment may be determined. The reluctance specification process is repeated as the rotor progresses under the coil group and is completed once the new

rotor position is  $\pi$  radians from where it was when the specification began.

The specification of the reluctance using this method is very simple. However, insight is required in the choice of the phase voltage wave shape. After the trailing edge of the rotor pole face passes the first slot, the reluctance specification is complete. The phase voltage and the required magnetic flux density must come from the remaining MMF time variation and the reluctance specified to this point.

#### Example

See Appendix I (Generator Design) for a reference on the generator specifications used in this example.

The proof that not just any phase voltage wave shape will work is seen by examination of the example developed so far. Table 5 gives the time variation of the total MMF at each slot for the Figure 5 voltage variation. At  $\omega t = -5\pi/15$ , none of the pole arc is under the phase C coil group. At  $\omega t = -4\pi/15$ , the pole will be under the first conductor of the coil group.

The MMF at  $\omega t = -4\pi/15$  is negative. Additional rotor MMF could be added here in order to ensure a positive magnetic flux density with a realizable reluctance. However, there is another difficulty. The desired magnetic flux density and therefore the desired voltage wave shape is flat between  $\omega t = -2\pi/15$  and  $\omega t = +3\pi/15$ . At  $\omega t = -2\pi/15$ , a certain combination of reluctances will be under slots 1, 2, and 3 and with the MMFs

(Table 5 entries) will produce the desired magnetic flux density. However, at  $\omega t = -\pi/15$ , the reluctances are exposed to greater MMFs. The new increment under slot 1 also sees a positive MMF. Then the reluctances which provide the correct amount of flux density at  $\omega t = -2\pi/15$  are bound to provide too much at  $\omega t = -\pi/15$ . Therefore, this choice of a phase voltage wave shape is not consistent for wave shape control using only rotor geometry.

#### Triangular Phase Voltage Wave Shape Example

The flexibility of the phase voltage wave shape for a required load voltage wave shape as discussed in Section III is valuable. Figure 9 shows a phase voltage wave shape which produces a DC load voltage. Notice that it has an upward ramping voltage as the number of slots with finite reluctances increases and a downward ramping voltage as the number of slots with finite reluctances decreases. In this example, the peak phase voltage equals the load voltage and the pole arc is only  $\pi/3$  electrical radians. Tables 7, 8, and 9 display the voltage, the magnetic flux density, the current, and the MMF variation at each slot versus time.

The reluctance for this new wave shape is introduced under the first conductor at  $\omega t = -3\pi/30$ . The rotor pole is centered under phase C at  $\omega t = -5\pi/30$ . It is under only one conductor at  $\omega t = 13\pi/30$  as it is leaving the coil group.

Table 10 shows the progressive calculation of the reluctances required for the Figure 9a triangular voltage wave shape. Notice that Table 10 stops with the determination that a negative reluctance is required. A rotor MMF of 1400 ampere-turns was chosen instead of the 533 ampere-turns used previously in order to prevent the calculation of a negative reluctance for the very first entry. This wave shape choice is not appropriate for rotor geometry control.

From the shaded area of Table 9, it is observed that an equation for the magnetic flux density (similar to Equation 39) may be written for each line (at each time increment). Nine equations with the specified MMF determine the required reluctances. Yet, only five reluctances are variable. The armature current and rotor MMF provide two additional variables. It is clear that design using the method of this section is a form of over-specification. There might be a waveform that fits all of the equations and provides the desired load voltage, but none were found.

Table 7 Normalized Phase Current and Voltage  
 (Triangle Wave Shape) (Figure 9a)

TIME ( $\omega t$ )	VOLTAGE			CURRENT		
	A	B	C	A'	B'	C'
- $5\pi/30$	0	1	0	-1	0	1
- $3\pi/30$	0	.8	-.2	-1	.36	.96
$-\pi/30$	0	.6	-.4	-1	.64	.84
$\pi/30$	0	.4	-.6	-1	.84	.64
$3\pi/30$	0	.2	-.8	-1	.96	.36
$5\pi/30$	0	0	1	-1	1	0
$7\pi/30$	.2	0	-.8	-.96	1	-.36
$9\pi/30$	.4	0	-.6	-.84	1	-.64
$11\pi/30$	.6	0	-.4	-.64	1	-.84
$13\pi/30$	.8	0	-.2	-.34	1	-.96
$15\pi/30$	1	0	0	0	1	-1
$17\pi/30$	.8	-.2	0	.34	.96	-1
$19\pi/30$	.6	-.4	0	.64	.84	-1
$21\pi/30$	.4	-.6	0	.84	.64	-1
$23\pi/30$	.2	-.8	0	.96	.36	-1
$25\pi/30$	0	1	0	1	0	-1

Table 8 Normalized Armature Reaction MMF Phase C Slots (Triangle Wave Shape)

TIME ( $\omega t$ ) \ X	$\pi/30$	$3\pi/30$	$5\pi/30$	$7\pi/30$	$9\pi/30$
$-5\pi/30$	-1.80	-1.40	-1.00	-.60	-.20
$-3\pi/30$	-2.13	-1.74	-1.36	-.98	-.59
$-\pi/30$	-2.31	-1.98	-1.64	-1.30	-.97
$\pi/30$	-2.35	-2.09	-1.84	-1.58	-1.33
$3\pi/30$	-2.25	-2.10	-1.96	-1.82	-1.67
$5\pi/30$	-2.00	-2.00	-2.00	-2.00	-2.00
$7\pi/30$	-1.67	-1.82	-1.96	-2.10	-2.25
$9\pi/30$	-1.33	-1.58	-1.84	-2.10	-2.35
$11\pi/30$	-.97	-1.30	-1.64	-1.98	-2.31
$13\pi/30$	-.57	-.96	-1.34	-1.72	-2.11
$15\pi/30$	-.20	-.60	-1.00	-1.40	-1.80
$17\pi/30$	.18	-.22	-.62	-1.02	-1.42
$19\pi/30$	.60	.20	-.20	-.60	-1.00
$21\pi/30$	1.00	.60	.20	-.20	-.60
$23\pi/30$	1.40	1.00	.60	2.00	-.20
$25\pi/30$	1.80	1.40	1.00	.60	.20

Table 9 Total MMF at Phase C Slots (Triangle Wave Shape)

TIME ( $\omega t$ )	x	$\pi/30$	$3\pi/30$	$5\pi/30$	$7\pi/30$	$9\pi/30$
$-5\pi/30$		-1129.59	-878.57	-627.55	-376.53	-125.51
$-3\pi/30$		63.32	-1091.94	-853.47	-615.00	-370.25
$-\pi/30$		-49.64	157.45	-1029.18	-815.81	-608.72
$\pi/30$		-74.74	88.42	245.31	-991.53	-834.64
$3\pi/30$		-11.99	82.14	170.00	257.86	-1048.00
$5\pi/30$		144.90	144.90	144.90	144.90	144.90
$7\pi/30$		-1048.01	257.86	170.00	82.14	-11.99
$9\pi/30$		-834.64	-991.53	245.31	82.14	-74.74
$11\pi/30$		-608.72	-815.81	-1029.18	157.45	-49.64
$13\pi/30$		-367.70	-602.45	-840.92	-1079.39	75.87
$15\pi/30$		-125.51	-376.53	-627.55	-878.57	-1129.59
$17\pi/30$		112.96	-138.06	-389.08	-640.10	-891.12
$19\pi/30$		376.53	125.51	-125.51	-376.53	-627.55
$21\pi/30$		627.55	376.53	125.51	-125.51	-376.53
$23\pi/30$		878.57	627.55	376.53	125.51	-125.51
$25\pi/30$		1129.59	878.57	627.55	376.53	125.51

Table 1 - Calculation of Incremental Reluctances (Triangle Wave Shape)

STAGE S	NUMBER N	KNOWN R AT SLOT					UNKNOWN R AT SLOT				B at 1	R at 1
		2	3	4	5	2	3	4	5	TOTAL		
1.5	1.0					.000	.000	.000	.000	.000	.000	x
1.5	2.5					.300	.000	.000	.000	.258	.258	2.45, 4.2
1.5	5.1	2.17, 4				.641	.000	.000	.000	.124	.124	5.8, 5.9
1.5	7.5	5.18, 6	2.15, 4			.222	1.600	.000	.000	1.221	.446	1.67, 4.4
1.5	10.5	1.67, 4	5.15, 4	2.15, 4		.491	.420	1.051	.000	1.967	.954	1.2, 8.4
1.5	12.5	1.67, 4	5.18, 6	2.15, 4	1.1, 2.8	.865	.565	.590	15.104	-11.812	-12.27	

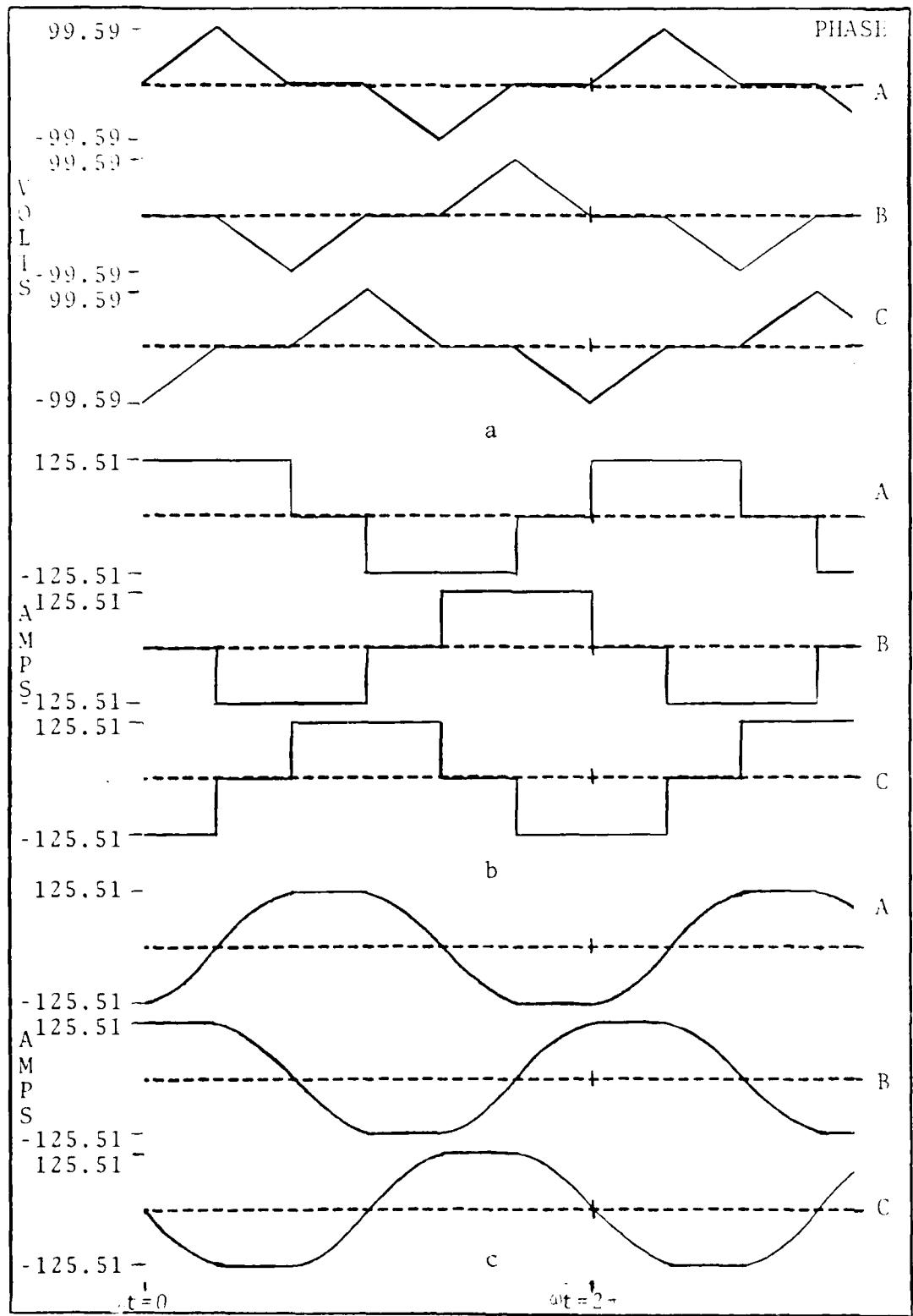


Figure 9 Triangle Phase Voltage and Current Wave Shapes

## X. Other Magnetic Effects

This section discusses the effects of flux leakage, flux fringing, and flux saturation on the desired generated voltage wave shape. Finite Element analysis, an important analytical tool, is introduced as a computer-aided design method used in fine tuning and checking the generator design. One example of a magnetic finite element analysis program is introduced.

### Introduction

All of the procedures, methods, and examples in this thesis effort assume zero flux leakage, no flux fringing, and no saturation in the generator's magnetic structure. These are important assumptions because calculating flux leakage, flux fringing, and saturation require a knowledge of the complete magnetic structure; something that is not available in the initial design stages. Generator design is by nature an iterative process due to these three problems.

When a generator is designed for a specific load, the system inductance is an important specification. The system inductance depends on the load inductance, the transmission line inductance, and also the generator inductance. The generator inductance can easily be the most significant of the three inductances. The generator inductance depends

on the geometry of the magnetic circuit. Designing the magnetic circuit, however, depends on a knowledge of the system inductance. Normally, a "first cut" design is made from which a "first cut" system inductance can be calculated. Using this inductance, a "second cut" design is made from which a "second cut" system inductance can be calculated. This process continues until it converges on a final design.

This thesis effort is concerned only with the "first cut" design. The rest of the design procedure is left for further study.

#### Leakage Flux

In the generator, the rotor magnetic flux is generated in the rotor coils. The flux travels through the rotor poles and into the stator magnetic structure cutting the armature coils and thus, generating the output voltage.

In a salient pole generator, there is a large air gap between two adjacent poles. The magnetic reluctance is very high, but does have a finite value. Since there is an MMF drop between two adjacent poles, there will be magnetic flux crossing the gap between the poles bypassing the stator. All of this leakage flux which bypasses the stator does not have a significant impact on the shape of the desired output voltage waveform, although it does increase the generator inductance,  $X_g$ . To compensate for

this leakage flux, all the designer needs to do is increase the number of ampere turns in the rotor coils.

### Fringing Flux

Another important assumption made in this thesis effort is that all the flux generated in the rotor passes through the air gap, past the armature coils and into the stator core in a totally radial direction. This is an important "first cut" assumption and can be corrected for in further design iterations.

In a realistic generator, the majority of the magnetic flux does go in the radial direction. However, there is a significant amount of flux which does not. This flux crosses the air gap in directions defined by the magnetic flux density vector  $\vec{B}$  causing a distortion of the desired output voltage wave shape. The flux can also short cut across several armature slots instead of going straight through.

Accounting and correcting for this fringing flux so that the correct flux links the armature coils is no simple matter. Where and how the flux fringes depends on the shape of the generator's magnetic structure. The correction for the flux fringing is therefore an iterative design process.

### Magnetic Saturation

The last important assumption made in this thesis effort is that the relationship between the MMF, the reluctance of the magnetic material, and the resultant flux density in the magnetic material is linear. This last assumption said another way means that the analysis in this thesis effort ignores the effects of saturation of the magnetic material.

In a realistic generator, this relationship is definitely non-linear. When the MMF dropped across the magnetic structure is a given value, a certain amount of magnetic flux will "flow" through the material. As the MMF increases, the flux flowing through the material also tends to increase. However, at high enough values of flux density, the magnetic material saturates and more and more MMF is required for smaller increases in the flux.

As was true for the flux fringing, the locations and the severity of the flux saturation are determined by the structure of the magnetic circuit. Compensating for this problem can also be an iterative design procedure.

### Finite Element Analysis

The calculations involved in designing a generator can be exceedingly complex and cumbersome. This fact makes the digital computer a welcome design aid. One particular procedure ideally suited for computer-aided design is Finite Element analysis.

In Finite Element analysis, a cross section of the generator is taken perpendicular to the axle. Then the assumption is made that any leakage flux or fringing flux is in the plane of the cross section. That is, there is no leakage flux or fringing flux between any two "adjacent, infinitely thin" cross sections. The two dimensional cross section is then divided up into triangular finite elements. Each element is restricted to one particular type of material (steel, air, insulation, ...). During the computations, each triangular finite element is considered to have a constant magnetic flux density over the entire element. See (Ref 8) and (Ref 13) for further information on the Finite Element method.

MAGNETIC is a computer program that uses the Finite Element analysis technique (Ref 4) to analyze magnetic structures. MAGNETIC computes the magnetic fields, induced currents and losses, and the forces of a magnetic device that has been represented as a collection of finite elements.

"MAGNETIC aids the design of magnetic devices because accurate prediction of devices performance usually requires knowledge of the magnetic field. MAGNETIC is a means of calculating the field that allows for fringing, saturation, permanent magnets, and complicated shapes. Because the program includes non-linear B-H curves and computes inductances, forces, and eddy current losses, it can help the designer to minimize the materials used in a device and maximize its efficiency." (Ref 4:11)

Two problems in generator design, flux fringing and saturation, force the design procedure to be iterative. MAGNETIC can be a welcome aid in correcting for flux fringing and saturation as well as flux leakage. After the designer has completed the "first cut" design, the design can be analyzed by MAGNETIC. MAGNETIC shows through its output, where and to what extent flux fringing, saturation, and flux leakage are occurring. With this information, the designer is able to take corrective action and come up with a "second cut" design. This procedure continues until an acceptable design is obtained.

In addition to tabular listings of the various output parameters, MAGNETIC produces a Mesh plot and a Flux plot. The Mesh plot portrays the selected generator cross section showing all the triangular finite elements. The Flux plot shows the lines of magnetic flux in the generator cross section. Figure 10 is the Mesh plot for the sample generator (Reference Appendix I). The Flux plot of the sample generator is not shown because that portion of MAGNETIC currently does not work.

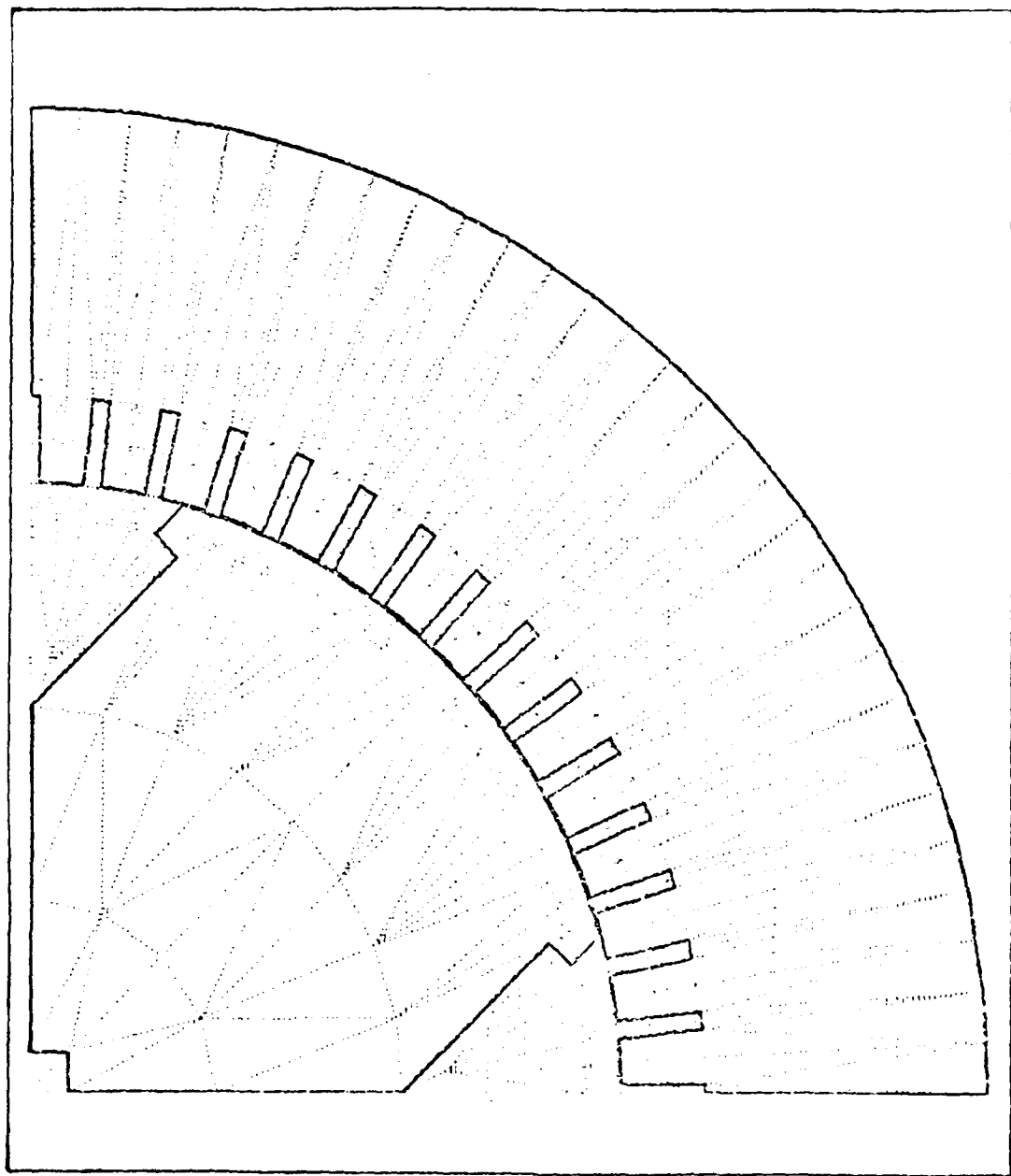


Figure 10 Sample Generator Mesh Plot

## XI. Conclusions and Recommendations

### Conclusions

The purpose of this thesis effort was to investigate the use of rotor geometry as a specification in the control of generator voltage and flux density harmonics. It was found that armature reaction MMF could be expressed as an infinite set of traveling waves with an infinite set of velocities (Section IV) and (Equation 23). Because the rotor MMF has only the velocity of the rotor, it cannot cancel armature reaction everywhere in the generator throughout all time (Section VII).

Rotor geometry was put to use in a limited control of flux density harmonics at the stator slots. The reflection of the MMFs present at all of the slots of a coil group into a single slot allows the possible calculation of an appropriate rotor geometry. This reflection turned out to exceed the resources of this thesis effort and was not accomplished (Section VIII).

Specifying the air gap reluctance incrementally as the rotor moves under successive stator slots was also tried as a means of harmonic control. This method was unworkable for all wave shapes chosen because it produced negative MMF requirements and conflicting geometry specifications.

### Recommendations

The control of flux density is an important consideration when working to improve generator efficiency and performance. Because of the potential that flux density control has, several recommendations for further study are presented.

Before any hardware is fabricated, it is recommended that the designer calculate the benefits due to the flux density control design. Knowing that energy is conserved between the input and the output of the generator, the designer will be able to calculate the design's value.

A recommended approach for reduction of losses is to investigate flux density control at the damper bars instead of the stator windings. This investigation however, will not control the generator output harmonics.

A different approach might be to use stator geometry as a design specification in harmonic control. This will not control the MMF at all time and all space by itself, but may provide easier control of the harmonics at a given location.

The method in Section VII could be further investigated if a method were derived for the division of one infinite series with progressive harmonic arguments by another such series. The Section VIII approach could be further investigated in terms of a general wave shape

(see the heading "The Contradiction" in Section VIII).

Either method might provide a workable wave shape or prove that the rotor geometry concept is in general impossible.

The general requirement for phase voltage wave shapes that produce a DC output from a three phase full wave bridge rectifier is:

$$\text{Voltage } (t) + \text{Voltage } \left(\frac{T_a}{2} + t\right) = \text{a constant} \quad (58)$$

where

$\text{Voltage } (t)$  is the wave shape during the first half of the period in which voltage is applied to the load

$\text{Voltage } \left(\frac{T_a}{2} + t\right)$  is the wave shape during the second half of the period in which voltage is applied to the load

$T_a$  is the period in which the phase voltage is applied to the load

$t$  is the time variable within the first half of the period  $T_a$

This could be a start in the exploration for a general phase voltage wave shape.

An additional recommendation is to investigate the shaping of rotor MMF using electronic control of the current in the rotor coils. This will aid in the shaping of the required flux density harmonics in the air gap.

The final recommendation is to include the flux fringing, flux leakage, and magnetic saturation problems in the calculation (only if the calculations are successful without these three problems) for the desired phase voltage wave shape. It should be recognized that the problem will now be iterative and Finite Element analysis (Section X) will be helpful.

### Bibliography

1. Adams, Arlon. Electromagnetics for Engineers. New York: Ronald Press Company, 1971.
2. Air Force Extension Course Institute. Course 54350 Generator and Control Equipment. Study Reference Guide Volume 2. Gunter AFB, Alabama, Air Training Command, April 1969. (54350-02-0869)
3. Appleyard, R. E. and William L. Ringland. "Alternating-Current Generators" in Standard Handbook for Electrical Engineers (Tenth Edition). Editor-In-Chief: Donald G. Fink. New York: McGraw-Hill, Inc., 1968.
4. Brauer, John R. Magnetic Handbook. Milwaukee, Wisconsin: A. O. Smith Corporation, May 1979.
5. Brockhurst, F. C., Professor of Electrical Engineering. Lecture materials distributed in EE 6.07, Electromechanical Components Design, School of Engineering, Air Force Institute of Technology, Wright-Patterson AFB, Ohio, 1980.
6. Erickson, William. Electrical Engineering Theory and Practice (Second Edition). New York: John Wiley & Sons, Inc., 1959.
7. Franklin, Paul W. Theory of the Three Phase Salient Pole Type Generator - Part I. Presented at the IEEE Winter Power Meeting. New York: January 30, 1972.
8. Huebner, Kenneth H. The Finite Element Method for Engineers. New York: John Wiley & Sons, Inc., 1975.
9. Jain, Gian Chand. Design, Operation, & Testing of Synchronous Machines. Bombay, India: Asia Publishing House, 1966.
10. Kreysig, Erwin. Advanced Engineering Mathematics (Fourth Edition). New York: John Wiley & Sons, Inc., 1979.
11. Krishnamurthy, K. A. "AC - DC and AC - AC Converter Control with Selective Reduction of Line Harmonics," IEE Proceedings, 125 (11): 1269-1270 (November 1978).

12. Shiling, W. J. "Exciter Armature Reaction and Excitation Requirements in a Brushless Rotating Rectifier Aircraft Generator," AIEE Transactions on Applications and Industry, 79 Part 2: 394-402 (1960).
13. Shugar, Theodore A. Mathematical Theory of the Finite Element Method - Some Introductory Aspects. TN number N-1552; Program numbers ER000-01-169. Civil Engineering Laboratory, Naval Construction Battalion Center, Port Hueneme, California, April 1979. (ADA070861)
14. Spiegel, M. R. Schaum's Outline of Theory and Problems of Fourier Analysis with Applications to Boundary Value Problems. New York: McGraw-Hill, Inc., 1974.

Appendix I Sample Generator

Specifications and Dimensions for  
the Sample Generator

## Appendix I Sample Generator

The development of the rotor geometry modification example in this thesis requires a constant air gap, salient pole, synchronous generator to begin the investigation. The generator selected is basically the one designed for the final exam in Air Force Institute of Technology course EE 6.07 (Electromagnetic Components Design, Spring, 1980). A few modifications are made due to thesis requirements. The design procedure for the sample generator is not presented. Specifications for the sample generator are presented in Table 11. A cross sectional drawing (perpendicular to the axle) of the generator is presented in Figure 11.

The design modifications developed in this thesis apply equally as well to any salient pole, synchronous generator as they do in the generator used to begin the investigation.

Notice that the generator design is in inches. All units shown in this appendix are converted to the MKS system for use in the body of this thesis.

AD-A100 813

AIR FORCE INST OF TECH WRIGHT-PATTERSON AFB OH SCHOO—ETC F/G 10/2  
THE EFFECT OF ROTOR GEOMETRY ON THE HARMONIC PERFORMANCE OF SYN—ETC(U)  
DEC 80 C STUERKE, D W NORDQUIST

UNCLASSIFIED

AFIT/GE/EE/80D-34

NL

2 OF 2  
AD-A  
10081A

END  
DATE FILMED  
7-81  
DTIC

Table 11  
Sample Generator Dimensions and Specifications

Machine Specifications

WYE connected three phase output  
460 volts RMS line to neutral phase voltage  
72.464 amperes RMS phase current  
Load power: 100 kilowatts  
Frequency: 400 hertz  
No rotor or stator vents  
Straight slot stator design  
60 slots  
4 poles  
0.015 inch constant air gap over the poles  
Synchronous speed: 12000 revolutions per minute  
Rotor tip speed: 393 feet per second  
Rotor MMF: 533 ampere turns per pole  
Maximum flux density: 1 Tesla  
Pole arc: 60 mechanical degrees,  $\alpha_p = 0.667$   
Rotor length: 25.347 inches  
Trancor "T" steel with 0.007 inch laminations  
Synchronous salient pole design

Winding Specifications

Six internally generated phases,  $m = 6$   
Armature conductors have no skew,  $K_{sv} = 1.0$   
 $q = 5$   
One series current path per output phase  
Full pitch stator winding,  $W/T_p = 1.0$ ,  $K_{pv} = \pm 1.0$   
Two layer lap design  
0.107 by 0.107 inch square conductors  
15000 amperes per square inch maximum current density  
80 volts per mil minimum insulation thickness  
 $T_p = 15$  slots

Assumptions (for "first cut" calculations)

Zero flux leakage  
Zero leakage reactance  
 $PF = 1.0$

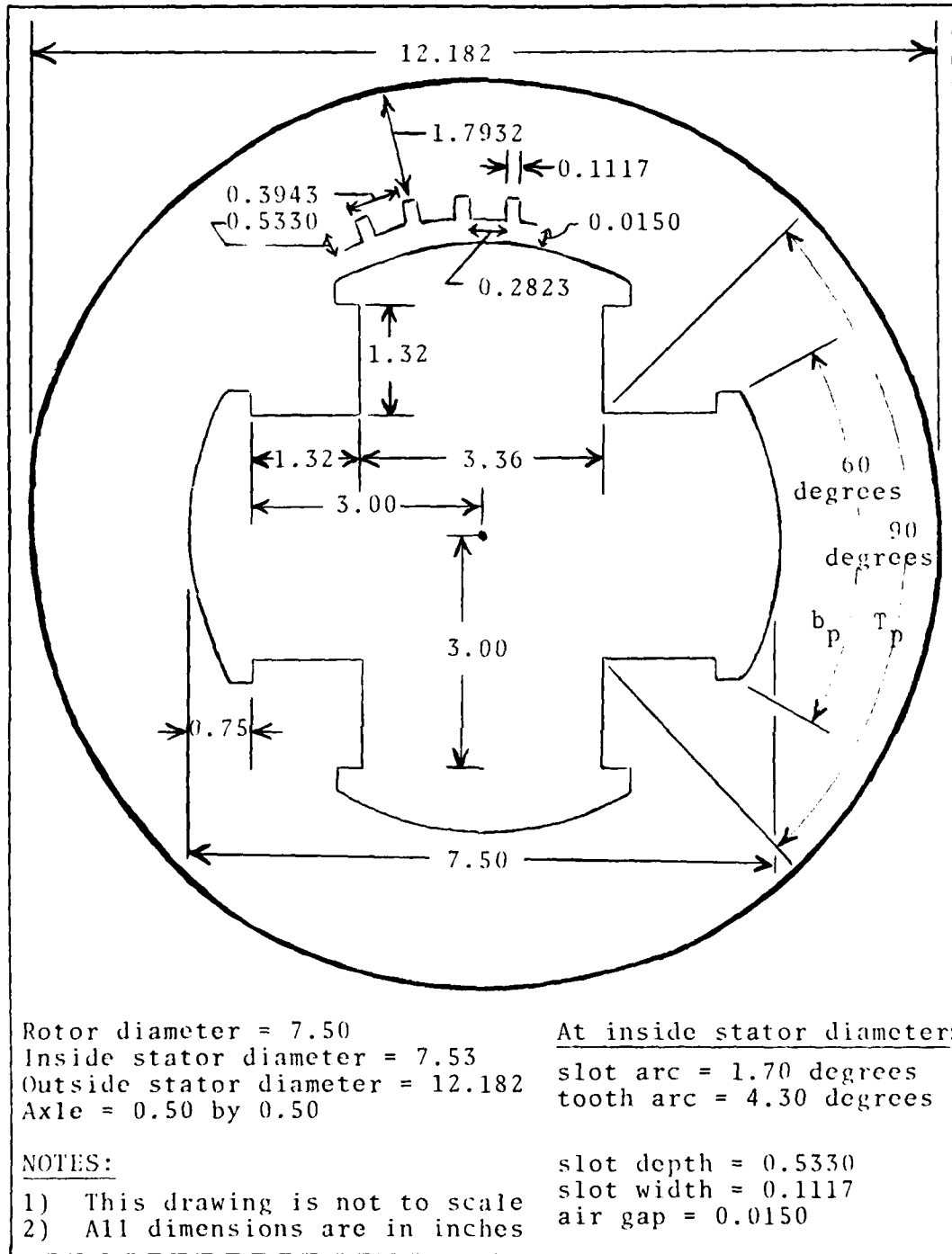


Figure 11 Cross Section of the Sample Generator  
(Specifications and Dimensions)

Appendix II RGRID and TRIA Card Generation

Computer Program to Generate RGRID and TRIA Cards  
Required by MAGNETIC (Ref 4) for the Air Gap and Pole  
Shoe Regions of the Sample Generator (Appendix I)

## Appendix II RGRID and TRIA Card Generation

The following program listing generates the RGRID and TRIA cards required by MAGNETIC (Ref 4) for the air gap and pole shoe regions of the sample generator (Appendix I).

Refer to Figure 12 and to the program listing for an explanation of how to use the program. Basically, to modify the program for another generator, the following must be accomplished:

- 1) Fill in the appropriate numbers in the three data statements.
- 2) Calculate values for the theta and radial coordinates for the points A, B, C, and D.
- 3) Write a statement function that describes the surface of the pole shoe.

The internal program structure is not discussed because it is not important for the program's use.

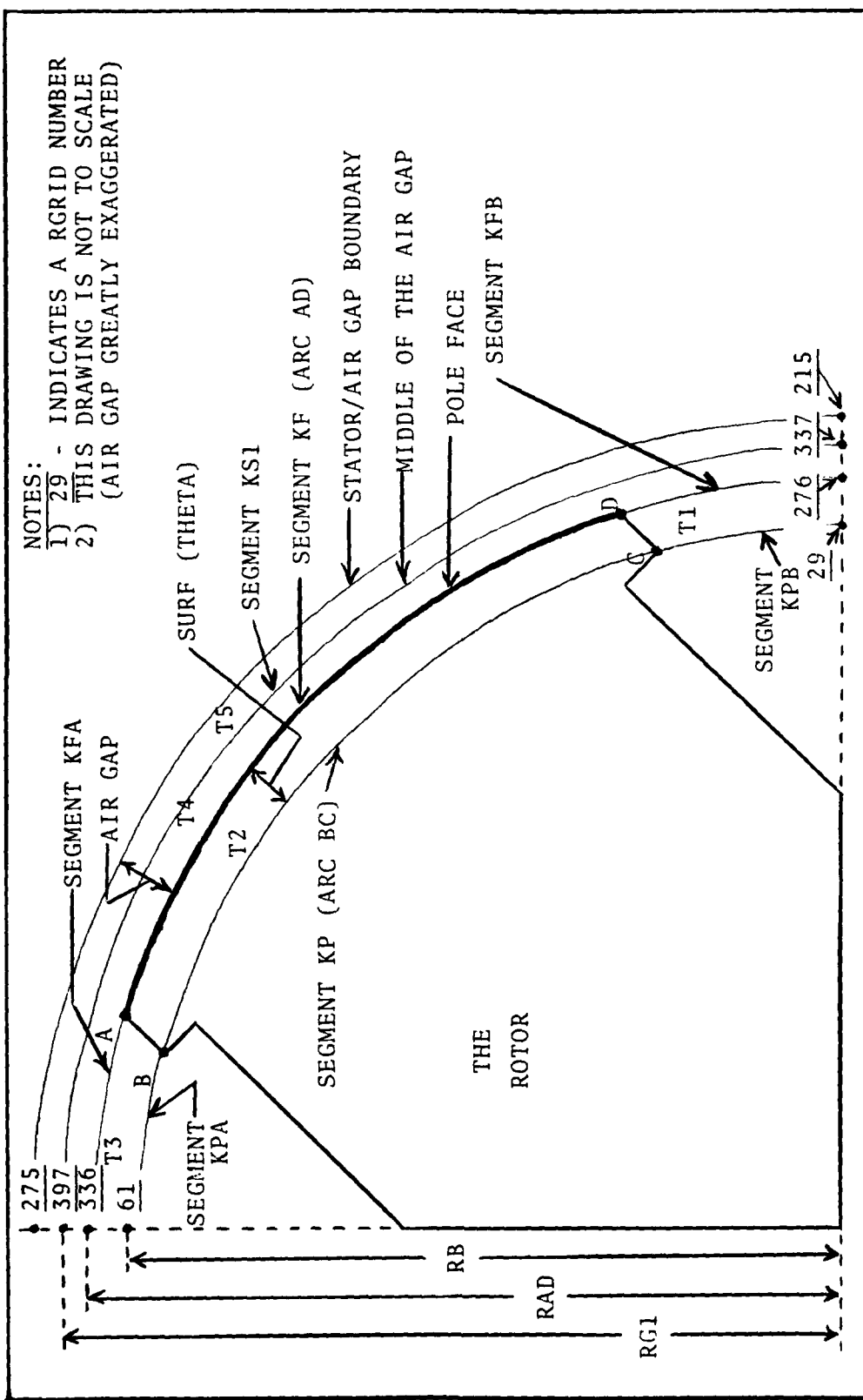


Figure 12 Cross Section of the Sample Generator (RGRID and TRIA Cards)

PROGRAM THESIS1 (INPUT,OUTPUT,PUNCH,TAPEE=OUTPUT,TAPE7=PUNCH)  
 C  
 C THIS PROGRAM GENERATES ONLY THE AIR GAP AND POLE SHOE RGRID  
 C AND TRIA CARDS REQUIRED BY THE PROGRAM MAGNETIC (REF 4) FOR  
 C THE SAMPLE GENERATOR  
 C  
 C VARIABLE DIMENSIONS  
 C  
 C ANG - ANGLE FOR INDIVIDUAL RGRID CARDS  
 C KEY - KEY=1 DESIGNATES A TRIA IS AIR, KEY=0 DESIGNATES STEEL  
 C LNG - LNG+1 = FIRST GRID NUMBER ASSIGNED  
 C LNS - LNS+1 = LOWEST GRID NUMBER ON THE STATION OF AIR GAP BOUNDARY  
 C LNT - LNT+1 = FIRST TRIA NUMBER ASSIGNED  
 C LPG - LPG+1 = FIRST GRID NUMBER ON THE RB ARC  
 C NF - NUMBER OF RGRID POINTS ON SEGMENT KF (INCLUDES THE ENDS)  
 C NFA - NUMBER OF RGRID POINTS ON SEGMENT KFA (INCLUDES THE ENDS)  
 C NFB - NUMBER OF RGRID POINTS ON SEGMENT KFB (INCLUDES THE ENDS)  
 C NG - RGRID NUMBER TO BE PUNCHED  
 C NG1 - NUMBER OF RGRID POINTS ON SEGMENT KG1 (INCLUDES THE ENDS)  
 C NP - NUMBER OF RGRID POINTS ON SEGMENT KP (INCLUDES THE ENDS)  
 C NPA - NUMBER OF RGRID POINTS ON SEGMENT KPA (INCLUDES THE ENDS)  
 C NPB - NUMBER OF RGRID POINTS ON SEGMENT KPB (INCLUDES THE ENDS)  
 C NT - TRIA NUMBER TO BE PUNCHED  
 C PI - CONSTANT 3.1415926535 ...  
 C RAD - RADIAL DISTANCE TO THE POLE FACE SURFACE  
 C RG1 - RADIAL DISTANCE TO THE MIDDLE OF THE AIR GAP  
 C  
 C XAB, XCC, XCD, XT, XY, XZ, AND YCC ARE USED TO CALCULATE  
 C THE COORDINATES FOR THE POINTS A, B, C, AND D.  
 C  
 C PA, RB, RC, AND RD ARE THE RADIAL COORDINATES OF A, B, C, AND D.  
 C TA, TB, TC, AND TD ARE THE THETA COORDINATES OF A, B, C, AND D.  
 C  
 C THE FOLLOWING VARIABLES ARE USED INTERNALLY IN THE PROGRAM ONLY:  
 C      DKTR      DNFP      DNFP4      DNFPB      DNGFM2      DNSG1  
 C      I      KB      KT      NFAM1      NFBM1      NFM1  
 C      NG1M1      NPAM1      NPB41      NPM1  
 C  
 C THE FOLLOWING ARE DESIGNATED LINE SEGMENTS - SEE FIGURE 12  
 C      KF      KFA      KFB      KG1      KP      KPA  
 C      KPB  
 C  
 C SUBROUTINES REQUIRED:  
 C      TRIA1 - PUNCHES TRIA CARDS FOR TYPE 1 FINITE ELEMENTS  
 C      TRIA2 - PUNCHES TRIA CARDS FOR TYPE 2 FINITE ELEMENTS  
 C SEE TRIA1 AND TRIA2 FOR FURTHER EXPLANATION.  
 C  
 C DOUBLE PRECISION TA,TB,TC,TD,RA,RB,RC,RD  
 C DOUBLE PRECISION ANG,RAD,PI  
 C DOUBLE PRECISION XY,XZ,XT,XCC,YCC,XCD,XAB

```

C
C DATA NFA,NF,NFR,NPA,NP,NPB,NG1,NS /11,41,11,6,23,6,61,61/
C DATA LNG,LNT,LPG,LNS /275,405,28,214/
C DATA RG1 /3.7575/
C
C THIS STATEMENT FUNCTION REPRESENTS THE SURFACE OF THE POLE
C SHOE. IT IS THE DISTANCE VERSUS X (THE ORIGIN IS IN THE
C CENTER OF THE POLE) ABOVE THE RB ARC. IN THIS CASE, A CONSTANT
C AIR GAP HAS BEEN SPECIFIED. THE ONLY RESTRICTION IS THAT THE
C POLE FACE MAY NOT HAVE ANY PORTIONS THAT ARE CONSTANT THETA
C LTNES.
C
C SURF(THETA)=1.21225707E47377357175475236D1
C
C 1010 FORMAT("1")
C 1011 FORMAT(" ", "RGRID", 5X, I3, 2(5X, F15.1))
C 1012 FORMAT("RGRID", 5X, I3, 2(5X, F15.1))
C
C GIVEN THE EQUATION FOR THE POLE SHOE SURFACE, CALCULATE THE
C COORDINATES FOR THE POINTS A, B, C, AND D.
C THE CONSTRAINTS ARE:
C 1) THE ARC LENGTH BETWEEN POINTS A AND B MUST BE 60
C MECHANICAL DEGREES.
C 2) THE LINE SEGMENTS AB AND DC MUST BE PARALLEL TO A
C LINE THROUGH THE CENTER OF THE GENERATOR DIVIDING
C THE POLE IN HALF.
C
C PI=3.141592653E897932834628433832795D0
C TA=75.0D0*PI/180.0D0
C TD=15.0D0*PI/180.0D0
C XY=DSQRT(.5D0+3.36D0*3.36D0)
C XZ=DSQRT(.5D0*1.32D0*1.32D0)
C XT=DSQRT(.5D0+0.195D0*0.195D0)
C XCC=XY+XZ+XT
C YCC=XZ-XT
C RC=DSQRT((XCC*XCC)+(YCC*YCC))
C R3=RC
C RA=SURF(TA)+RB
C RD=SURF(TD)+RB
C XAB=RA*DSIN(30.0D0*PI/180.0D0)
C TB=(45.0D0*PI/180.0D0)+DASIN(XAB/RB)
C XCD=R3*DSIN(30.0D0*PI/180.0D0)
C TC=(45.0D0*PI/180.0D0)-DASIN(XCD/RC)
C
C WRITE(6,1000)
C
C PUNCH THE RGRID CARDS.
C RGRID POINTS ARE TO BE EQUALLY SPACED ON GIVEN SEGMENTS.
C
C REMOVE THE C IN COLUMN 1 PRIOR TO ALL WRITE(7, ...) STATEMENTS

```

```

C IF PUNCHED CARD OUTPUT IS DESIRED.
C
C PUNCH RGRID CARDS FOR SEGMENT KPB - ONLY THE RIGHHAND END POINT
C
C     NG=LPG
C     NPM1=NPP-1
C     DO      1:    I=1,NPPM1
C             ANG=(TC/NPPM1)*(I-1)*(180.0D/PI)
C             NG=NG+1
C             WRITE(6,110) NG,RB,ANG
C             WRITE(7,120) NG,RB,ANG
C 10 CONTINUE
C
C PUNCH RGRID CARDS FOR SEGMENT KP - ONLY THE RIGHHAND END POINT
C
C     NPM1=NPP-1
C     DO      2:    I=1,NPM1
C             ANG=(TC+(((TB-TC)/NPM1)*(I-1)))*(180.0D/PI)
C             NG=NG+1
C             WRITE(6,110) NG,RB,ANG
C             WRITE(7,120) NG,RE,ANG
C 20 CONTINUE
C
C PUNCH RGRID CARDS FOR SEGMENT KPA - BOTH END POINTS
C
C     NPAM1=NPA-1
C     DO      3:    I=1,NPA
C             ANG=(TB+(((PI/2.0D)-TB)/NPAM1)*(I-1))*(180.0D/PI)
C             NG=NG+1
C             WRITE(6,110) NG,RB,ANG
C             WRITE(7,120) NG,RE,ANG
C 30 CONTINUE
C
C PUNCH RGRID CARDS FOR SEGMENT KFB - ONLY THE RIGHHAND END POINT
C
C     NG=LNG
C     NF3M1=NFB-1
C     DO      4:    I=1,NFBM1
C             ANG=(TD/NFBM1)*(I-1)*(180.0D/PI)
C             NG=NG+1
C             WRITE(6,110) NG,RD,ANG
C             WRITE(7,120) NG,RD,ANG
C 40 CONTINUE
C
C PUNCH RGRID CARDS FOR SEGMENT KF - BOTH END POINTS
C
C     NFM1=NF-1
C     DO      5:    I=1,NFM1
C             ANG=(TD+(((TA-TD)/NFM1)*(I-1)))*(180.0D/PI)
C             RAD=SURF(ANG)+RB

```

```

      NG=NG+1
      WRITE(6,101) NG,RAD,ANG
C      WRITE(7,102) NG,RAD,ANG
C      & CONTINUE
C
C PUNCH RGRID CARDS FOR SEGMENT KFA - BOTH END POINTS
C
      NFAM1=NFA-1
      DO      6   I=1,NFA
      ANG=((PI/2.0)-TA)/NFAM1*(I-1)*(180.0/PI)
      NG=NG+1
      WRITE(6,101) NG,RA,ANG
C      WRITE(7,102) NG,RA,ANG
C      & CONTINUE
C
C PUNCH RGRID CARDS FOR SEGMENT KG1 - BOTH END POINTS
C
      NG1M1=NG1-1
      DO      7   I=1,NG1
      ANG=((PI/2.0)/NG1M1)*(I-1)*(180.0/PI)
      NG=NG+1
      WRITE(6,101) NG,RG1,ANG
C      WRITE(7,102) NG,RG1,ANG
C      & CONTINUE
C
C ALL OF THE RGRID CARDS ARE NOW PUNCHED
C
C PROCEED TO PUNCH THE TRIA CARDS
C
C REMOVE THE C IN COLUMN 1 PRIOR TO ALL WRITE(7, ...) STATEMENTS
C IF PUNCHED OUTPUT IS DESIRED.
C
C PUNCH TRIA CARDS FOR REGION T1 (BETWEEN THE QUADRATURE AXIS
C AND THE RIGHT SIDE OF THE POLE SHOE
C
      KEY=1
      NT=LNT
      KT=1
      KB=1
      DNFBR=FLOAT(NFR)/FLOAT(NPB)
      80 DKTB=FLOAT(KT)/FLOAT(KB)
      IF (DKTB.GT.DNFBR)    GO TO 90
      IF (KT.EQ.NFB)        GO TO 100
      CALL TRIA1 (KT,KB,LNG,LPG,NT,KEY)
      GO TO 80
      90 CALL TRIA2 (KT,KB,LNG,LPG,NT,KEY)
      GO TO 80
C
C PUNCH TRIA CARDS FOR REGION T2. (THE POLE SHOE)
C

```

```

1 KEY=1
LNG=LNG+NFB-1
LPG=LPG+NFB-1
KT=1
KR=1
DNFP=FLCAT(NF)/FLOAT(NP)
11 DKT3=FLOAT(KT)/FLOAT(KR)
IF (DKT3.GT.DNFP) GO TO 12
IF (KT.EQ.NF) GO TO 13
CALL TRIA1 (KT,KR,LNG,LPG,NT,KEY)
GO TO 11
12 CALL TRIA2 (KT,KR,LNG,LPG,NT,KEY)
GO TO 11
C
3 PUNCH TRIA CARDS FOR REGION T3 (BETWEEN THE QUADRATURE AXIS
C AND THE LEFT SIDE OF THE POLE SHOE)
C
13 KEY=1
LNG=LNG+NF-1
LPG=LPG+NP-1
KT=1
KR=1
DNFPA=FLOAT(NFA)/FLOAT(NPA)
14 DKT3=FLOAT(KT)/FLCAT(KR)
IF (DKT3.GT.DNFPA) GO TO 15
IF (KT.EQ.NFA) GO TO 16
CALL TRIA1 (KT,KR,LNG,LPG,NT,KEY)
GO TO 14
15 CALL TRIA2 (KT,KR,LNG,LPG,NT,KEY)
GO TO 14
C
3 PUNCH TRIA CARDS FOR REGION T4. (LOWER HALF OF THE AIR GAP)
C
16 KEY=1
LNG=LNG+NFA
LPG=LNG-NFA-NF-NFB+2
KT=1
KR=1
DNGFM2=FLOAT(NG1)/FLOAT(NFA+NF+NFB-2)
17 DKT3=FLOAT(KT)/FLOAT(KR)
IF (DKT3.GT.DNGFM2) GO TO 18
IF (KT.EQ.NG1) GO TO 19
CALL TRIA1 (KT,KR,LNG,LPG,NT,KEY)
GO TO 17
18 CALL TRIA2 (KT,KR,LNG,LPG,NT,KEY)
GO TO 17
C
3 PUNCH TRIA CARDS FOR REGION T5. (UPPER HALF OF THE AIR GAP)
C
19 KEY=1

```

```
LNG=LNS  
LPG=LPG+(NFA+NF+NFB-2)  
KT=1  
KR=1  
DNG1=FLOAT(NS)/FLOAT(NG1)  
21 DKTB=FLOAT(KT)/FLOAT(KR)  
IF (DKTB.GT.DNG1) GO TO 21  
IF (KT.EQ.NS) GO TO 22  
CALL TRIA1 (K1,KR,LNG,LPG,NT,KEY)  
GO TO 24  
24 CALL TRIA2 (K1,KR,LNG,LPG,NT,KEY)  
GO TO 24  
22 STOP  
END
```

```

C THIS SUBROUTINE PUNCHES TRIA CARDS FOR TYPE 1 FINITE ELEMENTS.
C SEE THESTS1 FOR AN EXPLANATION OF ALL VARIABLES.
C REMOVE THE C IN COLUMN 1 PRIOR TO ALL WRITE(7, ...) STATEMENTS
C IF PUNCHED OUTPUT IS DESIRED.
C
C TYPE 1 FINITE ELEMENTS ARE TRIANGLES WITH DOWNWARD POINTING
C APEXES.
C
C      SUBROUTINE TRIA1 (KT,KR,LNG,LPG,NT,KEY)
N2=KT+LNG
N1=N2+1
N3=K3+LPG
KT=KT+1
NT=NT+1
IF (KEY.EQ.1)      GO TO 20
WRITE(6,111) NT,N1,N2,N3
C      WRITE(7,111) NT,N1,N2,N3
1011 FORMAT(" ", "TRIA", 4(5X,I3))
1111 FORMAT("TRIA", 4(5X,I3))
      RETURN
C
      21 WRITE(6,121) NT,N1,N2,N3
C      WRITE(7,121) NT,N1,N2,N3
1021 FORMAT(" ", "TRIA", 4(5X,I3),5X,"AIR")
1121 FORMAT("TRIA", 4(5X,I3),5X,"AIR")
      RETURN
END

```

```

C THIS SUBROUTINE PUNCHES TRIA CARDS FOR TYPE 2 FINITE ELEMENTS.
C SEE THESIS1 FOR AN EXPLANATION OF ALL VARIABLES.
C REMOVE THE C IN COLUMN 1 PRIOR TO ALL WRITE(7,...) STATEMENTS
C IF PUNCHED OUTPUT IS DESIRED.
C
C TYPE 2 FINITE ELEMENTS ARE TRIANGLES WITH UPWARD POINTING
C AFFEXES.
C
      SUBROUTINE TR1A2 (KT,KB,LNG,LPG,NT,KEY)
      N1=KT+LNG
      N2=KB+LPG
      N3=N2+1
      KB=KB+1
      NT=NT+1
      IF (KEY.EQ.1)      GO TO 20
      WRITE(5,111) NT,N1,N2,N3
C      WRITE(7,111) NT,N1,N2,N3
      111 FORMAT(" ","TRIA",4(5X,I3))
      111 FORMAT("TRIA",4(5X,I3))
      RETURN
C
      20 WRITE(5,121) NT,N1,N2,N3
C      WRITE(7,121) NT,N1,N2,N3
      121 FORMAT(" ","TRIA",4(5X,I3),5X,"AIR")
      121 FORMAT("TRIA",4(5X,I3),5X,"AIR")
      RETURN
      END

```

RGRID	29	3.5377+23245	6.6000000000
RGRID	30	3.5377+23245	2.5989233584
RGRID	31	3.5377+23245	5.1978467108
RGRID	32	3.5377+23245	7.7967710751
RGRID	27	3.5377+23245	1.0390634375
RGRID	33	3.5377+23245	12.9946157913
RGRID	28	3.5377+23245	1.04501971036
RGRID	29	3.5377+23245	18.8137773772
RGRID	30	3.5377+23245	21.1233570565
RGRID	31	3.5377+23245	24.6329379592
RGRID	32	3.5377+23245	27.5425182511
RGRID	40	3.5377+23245	31.4521985418
RGRID	41	3.5377+23245	33.3616766374
RGRID	42	3.5377+23245	36.2712591251
RGRID	43	3.5377+23245	39.1918394167
RGRID	44	3.5377+23245	42.6904197084
RGRID	45	3.5377+23245	45.0000000000
RGRID	46	3.5377+23245	47.9095302915
RGRID	47	3.5377+23245	51.8191605833
RGRID	48	3.5377+23245	53.7287406743
RGRID	49	3.5377+23245	56.6333211065
RGRID	50	3.5377+23245	59.5479014592
RGRID	51	3.5377+23245	52.4574817493
RGRID	52	3.5377+23245	55.3670620415
RGRID	53	3.5377+23245	58.2766123332
RGRID	54	3.5377+23245	71.1662226248
RGRID	55	3.5377+23245	74.6958029164
RGRID	56	3.5377+23245	77.0053832081
RGRID	57	3.5377+23245	79.0043055565
RGRID	58	3.5377+23245	82.2032293243
RGRID	59	3.5377+23245	84.6021532832
RGRID	60	3.5377+23245	87.4010766415
RGRID	51	3.5377+23245	91.0000000000
RGRID	276	3.7500000000	2.3000000000
RGRID	277	3.7500000000	1.5000000000
RGRID	278	3.7500000000	3.0000000000
RGRID	279	3.7500000000	4.5000000000
RGRID	280	3.7500000000	6.0000000000
RGRID	281	3.7500000000	7.5000000000
RGRID	282	3.7500000000	9.0000000000
RGRID	283	3.7500000000	10.5000000000
RGRID	284	3.7500000000	12.0000000000
RGRID	285	3.7500000000	13.5000000000
RGRID	286	3.7500000000	15.0000000000
RGRID	287	3.7500000000	16.5000000000
RGRID	288	3.7500000000	18.0000000000
RGRID	289	3.7500000000	19.5000000000
RGRID	290	3.7500000000	21.0000000000
RGRID	291	3.7500000000	22.5000000000
RGRID	292	3.7500000000	24.0000000000

RGRID	293	3.7500000000	25.5000000000
RGRID	294	3.7500000000	27.0000000000
RGRID	295	3.7500000000	28.5000000000
RGRID	296	3.7500000000	30.0000000000
RGRID	297	3.7500000000	31.5000000000
RGRID	298	3.7500000000	33.0000000000
RGRID	299	3.7500000000	34.5000000000
RGRID	300	3.7500000000	36.0000000000
RGRID	301	3.7500000000	37.5000000000
RGRID	302	3.7500000000	39.0000000000
RGRID	303	3.7500000000	40.5000000000
RGRID	304	3.7500000000	42.0000000000
RGRID	305	3.7500000000	43.5000000000
RGRID	306	3.7500000000	45.0000000000
RGRID	307	3.7500000000	46.5000000000
RGRID	308	3.7500000000	48.0000000000
RGRID	309	3.7500000000	49.5000000000
RGRID	310	3.7500000000	51.0000000000
RGRID	311	3.7500000000	52.5000000000
RGRID	312	3.7500000000	54.0000000000
RGRID	313	3.7500000000	55.5000000000
RGRID	314	3.7500000000	57.0000000000
RGRID	315	3.7500000000	58.5000000000
RGRID	316	3.7500000000	60.0000000000
RGRID	317	3.7500000000	61.5000000000
RGRID	318	3.7500000000	63.0000000000
RGRID	319	3.7500000000	64.5000000000
RGRID	320	3.7500000000	66.0000000000
RGRID	321	3.7500000000	67.5000000000
RGRID	322	3.7500000000	69.0000000000
RGRID	323	3.7500000000	70.5000000000
RGRID	324	3.7500000000	72.0000000000
RGRID	325	3.7500000000	73.5000000000
RGRID	326	3.7500000000	75.0000000000
RGRID	327	3.7500000000	76.5000000000
RGRID	328	3.7500000000	78.0000000000
RGRID	329	3.7500000000	79.5000000000
RGRID	330	3.7500000000	81.0000000000
RGRID	331	3.7500000000	82.5000000000
RGRID	332	3.7500000000	84.0000000000
RGRID	333	3.7500000000	85.5000000000
RGRID	334	3.7500000000	87.0000000000
RGRID	335	3.7500000000	88.5000000000
RGRID	336	3.7500000000	90.0000000000
RGRID	337	3.7575000000	1.0000000000
RGRID	338	3.7575000000	1.5000000000
RGRID	339	3.7575000000	3.0000000000
RGRID	340	3.7575000000	4.5000000000
RGRID	341	3.7575000000	6.0000000000
RGRID	342	3.7575000000	7.5000000000

RGRID	343	3.7575.00.000	9.0000000000
RGRID	344	3.7575.00.000	10.5000000000
RGRID	345	3.7575.00.000	12.0000000000
RGRID	346	3.7575.00.000	13.5000000000
RGRID	347	3.7575.00.000	15.0000000000
RGRID	348	3.7575.00.000	16.5000000000
RGRID	349	3.7575.00.000	18.0000000000
RGRID	350	3.7575.00.000	19.5000000000
RGRID	351	3.7575.00.000	21.0000000000
RGRID	352	3.7575.00.000	22.5000000000
RGRID	353	3.7575.00.000	24.0000000000
RGRID	354	3.7575.00.000	25.5000000000
RGRID	355	3.7575.00.000	27.0000000000
RGRID	356	3.7575.00.000	28.5000000000
RGRID	357	3.7575.00.000	30.0000000000
RGRID	358	3.7575.00.000	31.5000000000
RGRID	359	3.7575.00.000	33.0000000000
PGRID	360	3.7575.00.000	34.5000000000
RGRID	361	3.7575.00.000	36.0000000000
RGRID	362	3.7575.00.000	37.5000000000
RGRID	363	3.7575.00.000	39.0000000000
RGRID	364	3.7575.00.000	40.5000000000
RGRID	365	3.7575.00.000	42.0000000000
RGRID	366	3.7575.00.000	43.5000000000
RGRID	367	3.7575.00.000	45.0000000000
RGRID	368	3.7575.00.000	46.5000000000
RGRID	369	3.7575.00.000	48.0000000000
RGRID	370	3.7575.00.000	49.5000000000
RGRID	371	3.7575.00.000	51.0000000000
RGRID	372	3.7575.00.000	52.5000000000
RGRID	373	3.7575.00.000	54.0000000000
RGRID	374	3.7575.00.000	56.5000000000
RGRID	375	3.7575.00.000	57.0000000000
RGRID	376	3.7575.00.000	58.5000000000
RGRID	377	3.7575.00.000	60.0000000000
RGRID	378	3.7575.00.000	61.5000000000
RGRID	379	3.7575.00.000	63.0000000000
RGRID	380	3.7575.00.000	64.5000000000
RGRID	381	3.7575.00.000	66.0000000000
RGRID	382	3.7575.00.000	67.5000000000
RGRID	383	3.7575.00.000	69.0000000000
RGRID	384	3.7575.00.000	70.5000000000
RGRID	385	3.7575.00.000	72.0000000000
RGRID	386	3.7575.00.000	73.5000000000
RGRID	387	3.7575.00.000	75.0000000000
RGRID	388	3.7575.00.000	76.5000000000
RGRID	389	3.7575.00.000	78.0000000000
RGRID	390	3.7575.00.000	79.5000000000
RGRID	391	3.7575.00.000	81.0000000000
RGRID	392	3.7575.00.000	82.5000000000

RGRID	293	3.757500000	84.000000000
RGRID	294	3.757500100	85.500000000
RGRID	295	3.757500100	87.000000000
RGRID	296	3.757500100	88.500000000
RGRID	297	3.757500100	91.000000000
TRIA	310	277	AIR
TRIA	410	277	AIR
TRIA	411	278	AIR
TRIA	412	279	AIR
TRIA	413	279	AIR
TRIA	414	280	AIR
TRIA	415	281	AIR
TRIA	416	281	AIR
TRIA	417	282	AIR
TRIA	418	283	AIR
TRIA	419	283	AIR
TRIA	420	284	AIR
TRIA	421	285	AIR
TRIA	422	285	AIR
TRIA	423	285	AIR
TRIA	424	287	AIR
TRIA	425	287	AIR
TRIA	426	288	AIR
TRIA	427	288	AIR
TRIA	428	289	AIR
TRIA	429	289	AIR
TRIA	430	290	AIR
TRIA	431	291	AIR
TRIA	432	292	AIR
TRIA	433	293	AIR
TRIA	434	293	AIR
TRIA	435	294	AIR
TRIA	436	294	AIR
TRIA	437	295	AIR
TRIA	438	295	AIR
TRIA	439	295	AIR
TRIA	440	297	AIR
TRIA	441	298	AIR
TRIA	442	298	AIR
TRIA	443	299	AIR
TRIA	444	300	AIR
TRIA	445	300	AIR
TRIA	446	301	AIR
TRIA	447	302	AIR
TRIA	448	302	AIR
TRIA	449	303	AIR
TRIA	450	303	AIR
TRIA	451	304	AIR
TRIA	452	305	AIR
TRIA	453	305	AIR

TRIA	454	305	315	45
TRIA	455	307	315	45
TRIA	456	307	45	45
TRIA	457	303	317	46
TRIA	458	303	305	46
TRIA	459	303	45	47
TRIA	460	310	313	47
TRIA	461	310	47	48
TRIA	462	311	311	48
TRIA	463	312	311	48
TRIA	464	312	43	49
TRIA	465	313	312	49
TRIA	466	314	313	49
TRIA	467	314	49	50
TRIA	468	315	317	50
TRIA	469	315	315	50
TRIA	470	315	51	51
TRIA	471	317	316	51
TRIA	472	318	317	51
TRIA	473	318	51	52
TRIA	474	318	318	52
TRIA	475	319	52	53
TRIA	476	320	319	53
TRIA	477	321	320	53
TRIA	478	321	53	54
TRIA	479	322	321	54
TRIA	480	323	322	54
TRIA	481	323	54	55
TRIA	482	324	323	55
TRIA	483	325	324	55
TRIA	484	325	55	56
TRIA	485	325	325	56
TRIA	486	327	325	56
TRIA	487	327	56	AIR
TRIA	488	328	327	AIR
TRIA	489	328	328	AIR
TRIA	490	329	57	AIR
TRIA	491	331	329	AIR
TRIA	492	331	330	AIR
TRIA	493	331	53	AIR
TRIA	494	332	331	AIR
TRIA	495	333	332	AIR
TRIA	496	333	59	AIR
TRIA	497	334	333	AIR
TRIA	498	335	334	AIR
TRIA	499	335	53	AIR
TRIA	500	335	335	AIR
TRIA	501	339	337	276
TRIA	502	373	276	ATR
TRIA	503	339	338	AIR

TRIA	501	333	277	278	AIR
TRIA	505	340	339	278	AIR
TRIA	508	341	278	279	AIR
TRIA	507	361	347	279	AIR
TRIA	508	361	279	281	AIR
TRIA	509	367	271	281	AIP
TRIA	510	342	277	281	AIR
TRIA	511	363	342	281	AIR
TRIA	512	363	291	282	AIP
TRIA	513	344	343	282	AIR
TRIA	514	344	252	283	ATR
TRIA	515	345	344	283	AIR
TRIA	516	345	233	284	AIR
TRIA	517	365	345	284	AIR
TRIA	518	365	284	285	AIR
TRIA	519	347	346	285	AIR
TRIA	520	367	295	286	AIR
TRIA	521	363	347	286	AIR
TRIA	522	313	295	287	ATR
TRIA	523	340	343	287	AIR
TRIA	524	349	297	288	AIR
TRIA	525	360	349	288	AIR
TRIA	526	351	289	289	AIR
TRIA	527	351	351	289	AIR
TRIA	528	351	219	290	AIR
TRIA	529	352	351	291	AIR
TRIA	530	352	291	291	AIF
TRIA	531	353	352	291	AIR
TRIA	532	353	291	292	AIF
TRIA	533	354	353	292	AIR
TRIA	534	354	292	293	AIR
TRIA	535	355	354	293	AIR
TRIA	536	355	293	294	AIR
TRIA	537	355	353	294	AIR
TRIA	538	355	294	295	AIR
TRIA	539	357	356	295	AIR
TRIA	540	357	295	296	AIR
TRIA	541	358	357	296	AIR
TRIA	542	359	296	297	AIR
TRIA	543	359	359	297	AIR
TRIA	544	359	297	298	AIR
TRIA	565	361	359	298	AIR
TRIA	566	361	293	299	AIR
TRIA	567	361	357	299	AIF
TRIA	568	361	299	300	AIR
TRIA	569	362	351	300	AIR
TRIA	560	362	316	301	AIR
TRIA	561	363	362	301	AIR
TRIA	562	363	361	302	AIR
TRIA	563	364	363	302	AIP

TRIA	554	364	312	303	AIR
TRIA	555	365	364	303	AIR
TRIA	556	365	313	304	AIR
TRIA	557	365	365	304	AIR
TRIA	558	365	304	305	AIR
TRIA	559	367	366	305	AIR
TPIA	560	367	315	306	AIR
TRIA	561	368	367	306	AIR
TRIA	562	368	316	307	AIR
TRIA	563	369	363	307	AIR
TRIA	564	369	317	308	AIR
TRIA	565	370	369	308	AIR
TRIA	566	371	318	309	AIR
TRIA	567	371	370	309	AIR
TPIA	568	371	309	310	AIR
TRIA	569	372	371	310	AIR
TRIA	570	372	319	311	AIR
TRIA	571	373	372	311	AIR
TRIA	572	373	311	312	AIR
TRIA	573	374	373	312	AIR
TRIA	574	374	312	313	AIR
TRIA	575	375	374	313	AIR
TRIA	576	375	313	314	AIR
TRIA	577	375	375	314	AIR
TRIA	578	376	314	315	AIR
TRIA	579	377	376	315	AIR
TRIA	580	377	315	316	AIR
TRIA	581	378	377	316	AIR
TRIA	582	378	316	317	AIR
TRIA	583	379	378	317	AIR
TPIA	584	379	317	318	AIR
TRIA	585	380	379	318	AIR
TRIA	586	381	318	319	AIR
TRIA	587	381	301	319	AIR
TPIA	588	381	319	320	AIR
TRIA	589	382	331	320	AIR
TRIA	590	382	320	321	AIR
TRIA	591	383	332	321	AIR
TRIA	592	383	321	322	AIR
TRIA	593	384	333	322	AIR
TRIA	594	384	322	323	AIR
TRIA	595	385	334	323	AIR
TRIA	596	385	323	324	AIR
TRIA	597	386	331	324	AIR
TRIA	598	386	324	325	AIR
TRIA	599	387	390	324	AIR
TRIA	600	387	320	325	AIR
TRIA	601	388	387	325	AIR
TRIA	602	388	325	327	AIR
TRIA	603	389	388	327	AIR

TRIA	504	383	327	329	AIR
TRIA	505	390	389	328	AIR
TRIA	506	391	328	329	AIR
TRIA	507	301	331	329	AIR
TRIA	508	321	323	330	AIR
TRIA	509	322	321	331	AIR
TRIA	510	392	331	331	AIR
TRIA	511	393	332	331	AIR
TRIA	512	393	331	332	AIR
TRIA	513	394	333	332	AIR
TRIA	514	394	332	333	AIR
TRIA	515	395	394	333	AIR
TRIA	516	395	333	334	AIR
TRIA	517	395	395	334	AIR
TRIA	518	396	334	335	AIR
TRIA	519	397	396	335	AIR
TRIA	520	397	335	336	AIR
TRIA	521	215	215	337	AIR
TRIA	522	215	337	333	AIR
TRIA	523	217	215	338	AIR
TRIA	524	217	338	338	AIR
TRIA	525	218	217	339	AIR
TRIA	526	218	339	340	AIR
TRIA	527	218	218	340	AIR
TRIA	528	219	340	341	AIR
TRIA	529	221	219	341	AIR
TRIA	530	221	341	342	AIR
TRIA	531	221	220	342	AIR
TRIA	532	221	342	343	AIR
TRIA	533	222	221	343	AIR
TRIA	534	222	343	344	AIR
TRIA	535	223	222	344	AIR
TRIA	536	223	344	345	AIR
TRIA	537	224	223	345	AIR
TRIA	538	224	345	346	AIR
TRIA	539	225	224	346	AIR
TRIA	540	225	346	347	AIR
TRIA	541	226	225	347	AIR
TRIA	542	226	347	348	AIR
TRIA	543	227	226	348	AIR
TRIA	544	227	348	349	AIR
TRIA	545	228	227	349	AIR
TRIA	546	228	349	350	AIR
TRIA	547	228	223	351	AIR
TRIA	548	228	350	351	AIR
TRIA	549	231	229	351	AIR
TRIA	550	231	371	352	AIR
TRIA	551	231	230	352	AIR
TRIA	552	231	352	353	AIR
TRIA	553	232	231	353	AIR

TRIA	554	232	353	354	AIR
TRIA	555	233	352	354	AIR
TRIA	556	233	356	355	AIR
TRIA	557	234	353	355	AIR
TRIA	558	234	355	356	AIR
TRIA	559	235	357	357	AIR
TRIA	560	235	356	357	AIR
TRIA	561	235	357	357	AIR
TRIA	562	235	357	358	AIR
TRIA	563	237	358	359	AIR
TRIA	564	237	358	359	AIR
TRIA	565	238	357	359	AIR
TRIA	566	238	359	360	AIR
TRIA	567	239	359	361	AIR
TRIA	568	239	359	361	AIR
TRIA	569	241	360	361	AIR
TRIA	570	241	361	362	AIR
TRIA	571	241	361	362	AIR
TRIA	572	241	362	363	AIR
TRIA	573	242	361	363	AIR
TRIA	574	242	363	364	AIR
TRIA	575	243	362	364	AIR
TRIA	576	243	364	365	AIR
TRIA	577	244	363	365	AIR
TRIA	578	244	366	366	AIR
TRIA	579	245	366	366	AIR
TRIA	580	245	366	367	AIR
TRIA	581	245	367	367	AIR
TRIA	582	245	367	368	AIR
TRIA	583	247	366	368	AIR
TRIA	584	247	369	369	AIR
TRIA	585	248	367	369	AIR
TRIA	586	248	369	370	AIR
TRIA	587	248	368	370	AIR
TRIA	588	249	371	371	AIR
TRIA	589	251	371	371	AIR
TRIA	590	251	371	372	AIR
TRIA	591	251	371	372	AIR
TRIA	592	251	372	373	AIR
TRIA	593	252	371	373	AIR
TRIA	594	252	373	374	AIR
TRIA	595	253	372	374	AIR
TRIA	596	253	374	375	AIR
TRIA	597	254	373	375	AIR
TRIA	598	254	375	376	AIR
TRIA	599	255	374	376	AIR
TRIA	600	255	376	377	AIR
TRIA	601	255	375	377	AIR
TRIA	602	256	377	378	AIR
TRIA	603	257	375	378	AIR

TRIA	706	257	378	374	AIR
TRIA	715	259	257	373	AIR
TRIA	716	253	279	381	AIR
TRIA	717	252	273	381	AIR
TRIA	718	252	341	391	AIR
TRIA	719	254	271	381	AIR
TRIA	710	253	321	382	AIR
TRIA	711	251	261	362	AIR
TRIA	712	251	372	383	AIR
TRIA	713	252	251	382	AIR
TRIA	714	252	333	381	AIR
TRIA	715	253	252	384	AIR
TRIA	716	253	384	385	AIR
TRIA	717	254	253	385	AIR
TRIA	718	254	331	385	AIR
TRIA	719	255	264	385	AIR
TRIA	720	255	385	387	AIR
TRIA	721	255	255	387	AIR
TRIA	722	256	327	388	AIR
TRIA	723	257	256	388	AIR
TRIA	724	257	338	389	AIR
TRIA	725	258	267	389	AIR
TRIA	726	258	369	391	AIR
TRIA	727	259	269	391	AIR
TRIA	728	260	391	391	AIR
TRIA	729	271	259	391	AIR
TRIA	730	271	391	392	AIR
TRIA	731	271	271	392	AIR
TRIA	732	271	392	393	AIR
TRIA	733	272	271	393	AIR
TRIA	734	272	343	394	AIR
TRIA	735	273	272	394	AIR
TRIA	736	273	334	395	AIR
TRIA	737	274	273	395	AIR
TRIA	738	274	395	396	AIR
TRIA	739	275	274	395	AIR
TRIA	740	275	395	397	AIR

Vita

Cecil Stuerke was born 26 September 1949 in Sedalia, Missouri. He grew up in Kansas City, Kansas where he graduated from Wynadotte High School in 1967. He attended Kansas City, Kansas Community Junior College the following year. He then attended Kansas University from 1968 to 1971. Short of graduation, he enlisted in the United States Air Force. After serving one year at Richards Gerbaur Air Force Base, Grandview, Missouri, he returned to Kansas University under the Airman Education and Commissioning Program. He received Bachelor of Science Degrees in Electrical Engineering and Engineering Physics from Kansas University in 1975. He attended Officer's Training School and received an Air Force Commission on 24 March 1975. He was then assigned to the Air Force Aero-Propulsion Laboratory at Wright-Patterson Air Force Base until entering the School of Engineering, Air Force Institute of Technology in June 1979. He is a member of Eta Kappa Nu.

Permanent Address: 551 Westvale Road  
Kansas City, Kansas 66102

Vita

David W. Nordquist was born on 27 May 1952 in Chicago, Illinois. He graduated from Finneytown High School near Cincinnati, Ohio in 1970. He then attended the University of Cincinnati where he received, in 1975, the Degree of Bachelor of Science in Electrical Engineering. Shortly after graduation, he attended the Air Force Officer Training School where, in January 1976, he received his commission. He then served his first active duty assignment as a design engineer with the 6514th Test Squadron at Hill Air Force Base, Utah. He currently is assigned to the School of Engineering, Air Force Institute of Technology, Wright-Patterson Air Force Base, Ohio. He is a member of Eta Kappa Nu.

Permanent Address: 7715 Bluecrystal Court  
Cincinnati, OH 45224

## UNCLASSIFIED

SECURITY CLASSIFICATION OF THIS PAGE When Data Entered

REPORT DOCUMENTATION PAGE		READ INSTRUCTIONS BEFORE COMPLETING FORM
1. REPORT NUMBER AFIT/GE/EE/80D-34	2. GOVT ACCESSION NO. <i>AD-A100 813</i>	3. RECIPIENT'S CATALOG NUMBER
4. TITLE (and Subtitle) THE EFFECTS OF ROTOR GEOMETRY ON THE HARMONIC PERFORMANCE OF SYNCHRONOUS GENERATORS	5. TYPE OF REPORT & PERIOD COVERED MS Thesis	
7. AUTHOR(s) David W. Nordquist Captain	6. PERFORMING ORG. REPORT NUMBER	
9. PERFORMING ORGANIZATION NAME AND ADDRESS Air Force Institute of Technology Wright-Patterson Air Force Base, OH 45433	10. PROGRAM ELEMENT, PROJECT, TASK AREA & WORK UNIT NUMBERS	
11. CONTROLLING OFFICE NAME AND ADDRESS AF Wright Aeronautical Labs (POOS) Aeropropulsion Laboratory Wright-Patterson Air Force Base OH 45433	12. REPORT DATE December 1980	
14. MONITORING AGENCY NAME & ADDRESS (if different from Controlling Office)	13. NUMBER OF PAGES 121	
15. SECURITY CLASS. (of this report) <b>UNCLASSIFIED</b>		
16. DISTRIBUTION STATEMENT (of this Report) Approved for public release; distribution unlimited.		
17. DISTRIBUTION STATEMENT (of the abstract entered in Block 20, if different from Report)		
18. SUPPLEMENTARY NOTES Approved for public release; IAW AFR 190-17. <i>Fredric C. Lynch</i> 16 JUN 1981 FREDRIC C. LYNN, Major, USAF Director of Public Affairs		
19. KEY WORDS (Continue on reverse side if necessary and identify by block number) Synchronous Generators Generators Electric Generators Rotor Geometry		
20. ABSTRACT (Continue on reverse side if necessary and identify by block number) The use of rotor geometry as a specification in the control of generator voltage and flux density harmonics is studied. The possibility of generating a specific voltage waveform at the load with only a three-phase rectifier between the AC generator and the load is investigated.		

DD FORM 1 JAN 73 1473

EDITION OF 1 NOV 65 IS OBSOLETE

UNCLASSIFIED

SECURITY CLASSIFICATION OF THIS PAGE (When Data Entered)

**UNCLASSIFIED**

SECURITY CLASSIFICATION OF THIS PAGE WHEN DATA Entered

because the rotor MMF has only the velocity of the rotor.

The MMFs present at all the stator slots of an armature coil group are reflected into a single slot in an attempt to control the air gap flux density harmonics by selectively positioning increments of rotor reluctance. This method fails because a general solution for the reflected flux densities could not be obtained.

Specifying the air gap reluctance incrementally as the rotor moves under successive stator slots is also tried as a means of harmonic control. This method proves unworkable due to negative MMF requirements and conflicting geometry specifications.

Finite Element analysis is introduced as a computer aid to the design of a magnetic structure.

Recommendations for further study are included.

**UNCLASSIFIED**

SECURITY CLASSIFICATION OF THIS PAGE WHEN DATA Entered

